Systems/Circuits

Adenosinergic Modulation of Layer 6 Microcircuitry in the Medial Prefrontal Cortex Is Specific to Presynaptic Cell Type

Chao Ding,[1]* Danqing Yang,[1,2] and Dirk Feldmeyer[1,2,3]

[1]Research Center Juelich, Institute of Neuroscience and Medicine 10, Research Center Juelich, Juelich 52425, Germany, [2]Department of Psychiatry, Psychotherapy, and Psychosomatics, RWTH Aachen University Hospital, Aachen 52074, Germany, and [3]Jülich-Aachen Research Alliance, Translational Brain Medicine (JARA Brain), Aachen 52074, Germany

Adenosinergic modulation in the PFC is recognized for its involvement in various behavioral aspects including sleep homoeostasis, decision-making, spatial working memory and anxiety. While the principal cells of layer 6 (L6) exhibit a significant morphological diversity, the detailed cell-specific regulatory mechanisms of adenosine in L6 remain unexplored. Here, we quantitatively analyzed the morphological and electrophysiological parameters of L6 neurons in the rat medial prefrontal cortex (mPFC) using whole-cell recordings combined with morphological reconstructions. We were able to identify two different morphological categories of excitatory neurons in the mPFC of both juvenile and young adult rats with both sexes. These categories were characterized by a leading dendrite that was oriented either upright (toward the pial surface) or inverted (toward the white matter). These two excitatory neuron subtypes exhibited different electrophysiological and synaptic properties. Adenosine at a concentration of 30 μM indiscriminately suppressed connections with either an upright or an inverted presynaptic excitatory neuron. However, using lower concentrations of adenosine (10 μM) revealed that synapses originating from L6 upright neurons have a higher sensitivity to adenosine-induced inhibition of synaptic release. Adenosine receptor activation causes a reduction in the probability of presynaptic neurotransmitter release that could be abolished by specifically blocking A_1 adenosine receptors (A_1ARs) using 8-cyclopentyltheophylline (CPT). Our results demonstrate a differential expression level of A_1ARs at presynaptic sites of two functionally and morphologically distinct subpopulations of L6 principal neurons, suggesting the intricate functional role of adenosine in neuronal signaling in the brain.

Key words: **adenosine; cluster analysis; connectivity; layer 6; mPFC; neuromodulation**

Significance Statement

By performing unsupervised classification, we categorized the excitatory principal cells in layer 6 (L6) of the rat medial prefrontal cortex (mPFC) into two distinct morphological types: upright and inverted excitatory neurons. Our investigation revealed an abundant presence of inverted excitatory neurons in the rat mPFC, characterized by distinct morphological, electrophysiological and in particular synaptic properties. Our study expands earlier work on the inhibitory action of adenosine on synaptic transmission by demonstrating that when compared to inverted excitatory neurons, synapses formed by L6 upright neurons are more sensitive to adenosine. Our findings provide novel insight into the cell type-specific role of adenosine in neocortical modulation, unveiling the complex functional implications of layer 6 microcircuitry.

Introduction

Adenosine is a nearly ubiquitous endogenous neuromodulator involved in sleep homoeostasis and energy metabolism of neurons (Ribeiro et al., 2002; Porkka-Heiskanen and Kalinchuk, 2011). During prolonged wakefulness, hypoxia, ischemia or elevated metabolic demand, the extracellular adenosine concentrations can rise from nanomolar to micromolar levels indicating its critical role in both physiological and pathological CNS function (Dunwiddie

Received Aug. 25, 2023; revised Dec. 12, 2023; accepted Dec. 13, 2023.

Author contributions: C.D., D.Y., and D.F. designed research; C.D. and D.Y. performed research; C.D. and D.Y. analyzed data; C.D., D.Y., and D.F. wrote the paper.

We thank Werner Hucko for excellent technical assistance. We thank Dr. Karlijn van Aerde for custom-written macros in Igor Pro software. We warmly thank Prof. Andreas Bauer, Dr. Guanxiao Qi and Dr. Vishalini Emmenegger for helpful discussions. We are grateful for funding support from the European Union's Horizon 2020 Framework Programme for Research and Innovation under the Framework Partnership Agreement No. 650003 (HBP FPA) to D.F and China Scholarship Council (to C.D.).

The authors declare no competing financial interests.

*Present address: Synaptic Transmission in Energy Homeostasis Group, Max Planck Institute for Metabolism Research, Cologne 50931, Germany

Correspondence should be addressed to Danqing Yang at d.yang@fz-juelich.de or Dirk Feldmeyer at d.feldmeyer@fz-juelich.de.

https://doi.org/10.1523/JNEUROSCI.1606-23.2023

Copyright © 2024 Ding et al.

This is an open-access article distributed under the terms of the Creative Commons Attribution 4.0 International license, which permits unrestricted use, distribution and reproduction in any medium provided that the original work is properly attributed.

and Masino, 2001; van Calker and Biber, 2005; Fredholm, 2007). Among the four types of adenosine receptors, the A_1AR has the highest adenosine affinity and is the most abundant adenosine receptor type in the brain. It is densely expressed in the neocortex, particularly in layers 4 and 6 (Dunwiddie and Masino, 2001; Hackett, 2018). Acting via A_1AR, adenosine not only reduces the intrinsic excitability of glutamatergic neurons by increasing inwardly rectifying potassium conductance (Rainnie et al., 1994; Luscher et al., 1997) but also depresses excitatory neurotransmitter release by reducing presynaptic calcium influx and transmitter release (Wu and Saggau, 1994; Arrigoni et al., 2001; Kerkhofs et al., 2017; Qi et al., 2017). Therefore, the historical perspective has depicted adenosine as a primary inhibitory neuromodulator, exerting its function by suppressing neuronal activity through A_1ARs within the CNS. However, more recent research has revealed that adenosine also plays a pivotal role in augmenting excitatory synaptic transmission via acting A_{2A}ARs across many brain regions (Cunha and Ribeiro, 2000; Ciruela et al., 2006; Rebola et al., 2008; Simoes et al., 2016; Kerkhofs et al., 2018). While A_1ARs mainly contribute in shaping short-term synaptic plasticity, A_{2A}ARs are more engaged in modulating long-term potentiation (d'Alcantara et al., 2001; Costenla et al., 2011; Qi et al., 2017; Lopes et al., 2023). In light of this, adenosine is a neuromodulator that contributes to the precision of information processing mediated by a balanced activation of the inhibitory A_1 and the excitatory A_{2A}ARs.

The effects of adenosine on cortical neurons and networks across different brain regions have been well investigated (Lopes et al., 1999; Arrigoni et al., 2006; Yang et al., 2013; Bannon et al., 2014; van Aerde and Feldmeyer, 2015; Zhang et al., 2015; Qi et al., 2017). Heterogeneous modulation of adenosine has been found in the hippocampus, striatum, somatosensory cortex and cortico-striatal pathways, indicating its cell type-specific regulatory effects (Yoon and Rothman, 1991; Quiroz et al., 2009; Rombo et al., 2016; Qi et al., 2017). Cortical layer 6 excitatory neurons are known to exhibit a high degree of morphological diversity in many neocortical areas including the mPFC (Yang et al., 1996, 2022; Zhang and Deschênes, 1997; Kumar and Ohana, 2008; Thomson, 2010; Pichon et al., 2012; Marx and Feldmeyer, 2013; van Aerde and Feldmeyer, 2015). However, the intricate cell-specific regulatory mechanisms of adenosine within layer 6 (L6) have yet to be studied.

The role of adenosine in sleep homoeostasis is well documented. It has been shown that adenosine can promote and maintain sleep (Porkka-Heiskanen et al., 1997; Strecker et al., 2000; Basheer et al., 2004). Adenosine receptor antagonists such as caffeine can promote wakefulness and influence normal sleep patterns. Among many higher-order brain regions, the prefrontal cortex (PFC) is particularly sensitive to sleep and benefits from it in important ways (Oniz et al., 2019). Sleep deprivation leads to a loss of functional connectivity in the PFC and has a particular impact on brain functions that are mediated by the PFC, such as decreased working memory and increased irritability and apathy (Harrison et al., 2000; Verweij et al., 2014). In addition, it has been demonstrate that A_{2A}ARs play a regulatory role in the adenosinergic modulation of PFC activity and are involved in various behavioral aspects, such as decision-making, spatial working memory and anxiety (Caetano et al., 2017; Leffa et al., 2018; Li et al., 2018). To gain a more comprehensive understanding of the underlying mechanisms, it is crucial to investigate the adenosinergic modulation of synaptic transmission in the PFC.

Here, we performed quantitative classifications of excitatory neurons in L6 of rat medial PFC (mPFC) by using unsupervised cluster analysis (CA). Based on their dendritic morphology, two main clusters of L6 excitatory neurons were identified: (1) upright excitatory neurons with their leading or apical dendrites spanning superficial layers and (2) inverted/horizontally oriented excitatory neurons with their leading dendrites projecting toward the white matter or horizontally to it. Following this, we investigated the adenosinergic modulation of synaptic connections established by these L6 excitatory neuron types using paired patch clamp recordings with simultaneous biocytin fillings. We found that connections with presynaptic upright excitatory neurons were more sensitive to low concentrations of adenosine (10 μM) than connections with presynaptic inverted cells, although high concentrations of adenosine (30 μM) strongly suppressed all L6 excitatory connections via A_1AR activation. Our results revealed a cell type-specific effect of adenosine on the synaptic transmission in L6 excitatory microcircuits. This differential adenosine sensitivity may be involved in shifting the balance between subcortical and intracortical synaptic signaling.

Method and Materials

Slice preparation

All experimental procedures involving animals were performed in accordance with the guidelines of the Federation of European Laboratory Animal Science Association, the EU Directive 2010/63/EU, and the German animal welfare law. In this study, Wistar rats (Charles River, either sex) aged 17–21 postnatal days were obtained from Charles River and kept under a 12 h light/dark cycle, with food and water available ad libitum. Juvenile rats were housed in groups of 2–5 rats in a cage and rats older than 4 weeks were housed individually. Rats were maintained in a standard environment. Briefly, rats were deeply anesthetized with isoflurane and decapitated. The brain was quickly removed and placed in an ice-cold artificial cerebrospinal fluid (ACSF) containing 125 mM NaCl, 2.5 mM KCl, 1.25 mM NaH_2PO_4, 4 mM $MgCl_2$, 1 mM $CaCl_2$, 25 mM $NaHCO_3$, 25 mM glucose, 3 mM myo-inositol, 2 mM Na-pyruvate, and 0.4 mM ascorbic acid; the osmolarity of the solution was ~310 mOsm. The extracellular Ca^{2+} concentration was lowered to reduce potential excitotoxic synaptic transmission during slicing. In order to maintain adequate oxygenation and a physiological pH level, the solution was constantly bubbled with carbogen gas (95% O_2 and 5% CO_2). 350 μm thick coronal slices of the prelimbic mPFC were cut using a vibrating microslicer at a low speed and high vibration frequencies. The slices were then transferred to an incubation chamber for a recovery period of ~1 h at room temperature. Whole-cell patch-clamp recordings were made from submerged slices with continuous ACSF flowing in perfusion chamber at ~5 ml/min. This artificial CSF containing: 125 mM NaCl, 2.5 mM KCl, 1.25 mM NaH_2PO_4, 1 mM $MgCl_2$, 2 mM $CaCl_2$, 25 mM $NaHCO_3$, and 25 mM glucose, bubbled with carbogen gas and maintained at ~31°C. Patch pipettes were pulled from thick-wall borosilicate glass capillaries and filled with an internal solution containing 135 mM K-gluconate, 4 mM KCl, 10 mM HEPES, 10 mM phosphocreatine, 4 mM Mg-ATP, and 0.3 mM GTP (pH 7.4 with KOH, osmolarity ~300 mOsm). Biocytin (0.5%) was added to the internal solution to obtain permanent staining of the patched neurons for morphological analysis.

Cell identification

Slices were placed in the recording chamber under an upright microscope (equipped with 4× plan/0.13 numerical aperture and 40× water immersion/0.80 NA objectives; Olympus) with the pial surface facing forward. Cortical layers were distinguished by cell density and soma size, in accordance with previous studies on the PFC (Gabbott et al., 2005; van Aerde and Feldmeyer, 2015; Mitric et al., 2019; Ding et al., 2021). The PFC can be divided into three sections: the upper third comprises L1–L3, the middle third L5, and the lower third L6. Putative excitatory neurons and interneurons were differentiated based on their intrinsic action potential (AP) firing pattern during recording and their morphological appearance after post hoc histological staining. Interneurons were excluded from the analysis.

Electrophysiology

Whole-cell patch clamp recordings were made using an EPC10 amplifier (HEKA). Signals were sampled at 10 kHz, filtered at 2.9 kHz using Patchmaster software (HEKA), and later analyzed off-line using Igor Pro software (Wavemetrics). Recordings were performed using patch pipettes with a resistance of 6–10 MΩ. The resting membrane potential was measured immediately after establishing the whole-cell configuration. Bridge balance and capacitance neutralization were adjusted. The whole-cell series resistance was monitored throughout the experiment and was compensated by 80%. Membrane potentials were not corrected for the junction potential. Passive and active action potential properties were assessed by injecting a series of hyper- and depolarising, current pulses under current clamp configuration for 1 s. Dual whole-cell recordings were performed in L6 of the mPFC in order to record synaptically coupled neuron pairs. Due to the low intralaminar connectivity ratio in L6, a "searching" procedure was used to identify potential presynaptic neurons (Feldmeyer et al., 1999; Feldmeyer and Radnikow, 2016): Putative presynaptic neurons were randomly patched in "loose cell-attached" mode. When an AP elicited by a current pulse resulted in an excitatory postsynaptic potential (EPSP), this presynaptic neuron was repatched with a new pipette filled with biocytin-containing internal solution. The "searching" pipette (see below) was filled with an internal solution in which K^+ is replaced by Na^+ (containing [in mM]: 105 Na-gluconate, 30 NaCl, 10 HEPES, 10 phosphocreatine, 4 Mg-ATP, and 0.3 GTP) in order to prevent the depolarization of neighboring neurons during searching for a presynaptic cell. To obtain a low staining background of pre- and postsynaptic neurons, no biocytin was added to the Na-based internal solution in "searching" pipettes.

Drug application

Adenosine (10–100 μM), 8-Cyclopentyltheophylline (CPT, 1 μM), CGS21680 (30 nM), tetrodotoxin (TTX, 0.5 μM), and gabazine (10 μM) were all bath applied via the perfusion system for 3–7 min; drugs were purchased either from Sigma-Aldrich or Tocris.

Histological procedures

After single cell or paired-recordings, slices containing biocytin-filled neurons were fixed for at least 24 h at 4°C in 100 mM phosphate buffer solution (PBS, pH 7.4) containing 4% paraformaldehyde (PFA). After several rinses in PBS, slices were treated with 1% H_2O_2 in PBS for approximately 20 min, in order to quench endogenous peroxidase activity. Following this, slices were rinsed several times using 100 mM PBS and subsequently incubated in 1% avidin-biotinylated horseradish peroxidase (Vector ABC staining kit, Vector Lab. Inc.) containing 0.1% Triton X-100 for 1 h at room temperature. This was followed by a chromogenic reaction that resulted in a dark precipitate by adding 0.5 mg/ml 3,3-diaminobenzidine (DAB; Sigma-Aldrich) until distinct axonal and dendritic branches of the biocytin-filled neurons were clearly visible. The slices were rinsed again with 100 mM PBS, followed by slow dehydration in increasing ethanol concentrations and finally in xylene for 2–4 h. Slices were then mounted on gelatinized slides and embedded using Eukitt medium (Otto Kindler GmbH).

Morphological 3D reconstructions

Computer-assisted morphological 3D reconstructions of biocytin-filled L6 neurons were made using NEUROLUCIDA® software (Micro BrightField) and an Olympus BV61 microscope at 1,000× magnification (100× objective, 10× eyepiece). Neurons were selected for reconstruction based on the quality of biocytin labeling when background staining was minimal. The cell body, dendritic and axonal branches were reconstructed manually under constant visual inspection to detect thin and small collaterals. Layer borders, pial surface and white matter were delineated during reconstructions at lower magnification. The position of soma and layers were confirmed by superimposing the differential interference contrast images taken during the recording. The tissue shrinkage was corrected using correction factors of 1.1 in the x–y direction and 2.1 in the z direction (Marx et al., 2012).

Data analysis

Morphological properties. 3D reconstructed neurons were quantitatively analyzed using Neuroexplorer software (MicroBrightField) to determine morphological properties such as the dendritic length, the number of dendritic ends, the distribution of dendritic length in cortical layers 1–6 and the white matter, and the angle of the leading dendrite. Intersoma distances of synaptic coupled pairs were computed as the 3D-Euclidean distance between two somata. In acute brain slices, axonal collaterals, in particular those of principal cells are severely truncated during the cutting procedure (Egger et al., 2020). Therefore, in this study, the axonal properties of upright and inverted excitatory neurons were not included in the morphological analysis.

Unsupervised hierarchical CA. Dendritic morphological parameters were used for unsupervised CA. Parameters were standardized using z-score in order to make the distributions numerically comparable. The principal component analysis (PCA) was used to analyze the interdependence between variables and to reduce the dimensionality of the dataset while preserving maximum variability. PCA reduces the redundancy of the dataset by eliminating correlated variables and produces linear combinations of the original variables to generate new axes. To determine the number of principal components (PCs) to retain for CA, we used Kaiser's rule, an objective way to determine the number of clusters by leaving all components with eigenvalues <1. Since the dataset is standardized, the variables have an eigenvalue of 1, and hence, PCs with an eigenvalue >1 describe more of the data's variance than the original variable. Classification of excitatory neuron subtypes was then performed using unsupervised hierarchical CA employing Ward's method (Ward, 1963). Euclidean distance was used to calculate the variance. A dendrogram was constructed to visualize the distance at which clusters are combined.

Passive and active electrophysiological properties. Custom-written macros for Igor Pro 6 (Wavemetrics) were used for the analysis of the recorded electrophysiological data. Recordings with a series resistance exceeding 45 MΩ were excluded from the data analysis. The resting membrane potential (V_{rest}) of the neuron was measured directly after breakthrough into the whole-cell configuration with no current injection. To calculate the input resistance (R_{in}), the slope of the linear fit to the voltage step from −60 to −70 mV of the current–voltage relationship was used. The membrane time constant was calculated as monoexponential fit to the decay of the hyperpolarising voltage response after a current step of −50 pA. For the analysis of single spike characteristics such as threshold, amplitude, and half-width, a 10 pA step size increment for current injection was used to ensure that the action potential was elicited very close to its voltage threshold. The rheobase current was defined as the minimal current that elicited the first spike. The AP half-width was measured as the time difference between rising phase and decaying phase of the spike at half-maximum amplitude, and the AP amplitude was calculated as the difference in voltage from AP threshold to the peak during depolarization. The AP threshold was defined as the point of maximal acceleration of the membrane potential using the second derivative (d_2V/dt^2), i.e., the time point with the fastest voltage change, and the AP latency was defined as the time required for the onset of first AP in rheobase current stimulus. The AHP amplitude was calculated as the difference in voltage from AP threshold to maximum deflection of the repolarization. The current–frequency (If) plot was the slope of the linear fit of the current–frequency response curve between 0 and 300 pA. The interspike interval (ISI) was measured as the average time between individual spikes at a current step eliciting 10 APs. The adaptation ratio was measured as the ratio of the ninth ISI and the third ISI.

Synaptic properties. Synaptic properties were evaluated as described previously (Feldmeyer et al., 1999; Feldmeyer and Radnikow, 2016). All unitary EPSP (uEPSP) recordings were aligned to their corresponding presynaptic AP peaks, and an average sweep was generated as the mean uEPSP. The EPSP amplitude was calculated as the difference between the mean baseline and maximum voltage of the postsynaptic event. The paired-pulse ratio was defined as the second/third uEPSP divided by the first uEPSP amplitude elicited by presynaptic APs at a stimulation frequency of 10 Hz. Failures were defined as events with an amplitude <1.5× the SD of the noise within the baseline window; the failure rate refers to the percentage of failures. The coefficient of variation (CV) was calculated as the

SD divided by the mean uEPSP amplitude. Rise time was calculated as the mean time to rise from 20 to 80% of the peak amplitude. The latency was calculated as the time interval between the peak amplitude of presynaptic AP and the onset of the EPSP. The EPSP decay time was measured using a single exponential fit to the decay phase of both individual and averaged responses. The properties mentioned above were obtained from 20 to 80 successive sweeps.

Statistics. Data were either presented as box plots ($n \geq 10$) or as bar histograms ($n < 10$). For box plots, the interquartile range (IQR) is shown as a box, the range of values that are within 1.5 × IQR is shown as whiskers and the median is represent by a horizontal line in the box; for bar histograms, the mean ± SD is given. Wilcoxon Mann–Whitney *U* test was performed to assess the difference between individual clusters. Statistical significance was set at $p < 0.05$, and n indicates the number of neurons/connections analyzed.

Results

"Upright" and "inverted" excitatory neurons in layer 6 of mPFC

Excitatory neurons in layer 6 of the PFC have generally one main leading dendrite that projects either to the pia surface or toward the white matter (WM) or both. The projection pattern of this leading dendrites exhibits a high degree of heterogeneity, which is likely to have implications for their local synaptic connectivity and network function (Zhang and Deschênes, 1997; van Aerde and Feldmeyer, 2015; Yang et al., 2022). Here we have classified L6 excitatory neurons mainly on the basis of the structural properties of the main dendrite with reference to their projecting angles and cortical layer distributions (Table 1). The PCA was used to analyze the interdependence between variables to avoid double weighting of the correlated variables in the CA. The first three PCs with eigenvalues larger than one were retained for CA explaining 76% of the total variance. CA based on morphological parameters grouped 79 L6 excitatory neurons into two main clusters: 48 "upright" neurons (61%) with main dendrites projecting to the pia, spanning superficial layers and terminating in L5 to L1; 31 inverted/horizontally oriented neurons (39%) with a prominent main dendrite pointing to the WM or laterally oriented (Table 1). The two main clusters can be further subdivided into six sub-clusters (cluster 1) and two sub-clusters (cluster 2) (Fig. 1*B,C*). The optimal number of clusters was determined using the Thorndike method, where the cut-off points have the largest linkage distance.

Of the 48 upright excitatory neurons analyzed here, three were bipolar neurons, seven wide pyramidal-like neurons (PNs), two broad tufted PNs, 13 slender tufted PNs, eight untufted PNs and 15 short PNs. Bipolar spiny neurons have two major dendrites that are generally longer and thicker than the other dendrites and point toward the pial surface and the WM, respectively (Zhang and Deschênes, 1997). Here, the longest and thickest dendrite was considered as leading or principal dendrite because of its upright projection pattern, three bipolar neurons were classified into the "upright" neuron cluster. Wide neurons have long, sparsely tufted apical dendrites that extend as far as layer 1 and exhibit horizontally projecting basal dendrites. This dendritic morphology has been found to be typical of intratelencepalic (IT) claustrum-projecting PNs in layer 6 of the primary visual cortex (Katz, 1987; Cotel et al., 2018). Broad-tufted PNs, slender-tufted PNs, untufted PNs and short PNs were named based on their apical dendritic distribution in different cortical layers (Fig. 1*C,D*). Broad- and slender-tufted PNs had a tall apical dendrite that terminated close to the pial surface. A significant proportion of the apical dendritic tuft of these neurons was located in L1. The apical tuft had a large field span in the broad tufted PNs (763 ± 219 µm, $n = 2$ neurons) but was only narrow in the slender tufted PNs (343 ± 164 µm,

Table 1. Morphological and electrophysiological properties of excitatory neurons in L6 of rat mPFC

	Upright neurons	Inverted neurons	Mann–Whitney Test
Morphological properties	$n = 48$ for upright and $n = 31$ for inverted neurons		
Ends of dendrite	18.3 ± 7.9	13.6 ± 4.2	***0.0038***
Length of basal dendrites (µm)	2,412.5 ± 1,084.8	1624.7 ± 589.8	****0.0002***
Length of longest basal dendrite (µm)	842.6 ± 589.6	677.7 ± 456.7	***0.0436***
Angle of principal dendrite	93.3 ± 10.2	260.1 ± 41.3	*****8.73×10^{-11}***
Length of principle dendrite (µm)	3,097.5 ± 1,439.0	3,620.7 ± 945.5	***0.0436***
Length-P-dendrite in L1 (µm)	536.3 ± 938.3	0.0 ± 0.0	-
Length-P-dendrite in L2 (µm)	103.6 ± 130.9	0.0 ± 0.0	-
Length-P-dendrite in L3 (µm)	414.6 ± 390.5	0.0 ± 0.0	-
Length-P-dendrite in L5 (µm)	1,140.6 ± 538.8	33.2 ± 67.8	*****8.74×10^{-11}***
Length-P-dendrite in L6 (µm)	905.7 ± 588.3	2,106.2 ± 821.9	*****7.27×10^{-11}***
Length-P-dendrite in WM (µm)	3.5 ± 14.9	1,477.2 ± 828.0	*****3.50×10^{-11}***
Electrophysiological properties	$n = 20$ for upright and $n = 11$ for inverted neurons		
resting membrane potential (mV)	−66.8 ± 5.2	−60.5 ± 4.0	****0.0006***
Input resistance (MΩ)	192.4 ± 85.1	298.5 ± 117.9	*****4.64×10^{-5}***
Membrane time constant (ms)	25.4 ± 5.7	34.3 ± 7.5	***0.0025***
Rheobase current (pA)	112.5 ± 39.3	49.1 ± 13.0	*****5.5×10^{-7}***
AP half-width (ms)	1.05 ± 0.14	1.34 ± 0.16	*****7.6×10^{-5}***
AP amplitude (mV)	88.8 ± 8.2	83.8 ± 6.0	0.1229
AP threshold (mV)	−33.2 ± 4.5	−29.5 ± 3.2	***0.0292***
AHP amplitude (mV)	12.5 ± 3.9	15.0 ± 3.2	0.0539
AP latency (ms)	246.8 ± 191.4	325.8 ± 223.7	0.2608
frequency-current slope (Hz/100 pA)	15.9 ± 6.8	20.1 ± 3.9	***0.0364***
ISI average (ms)	90.2 ± 12.8	78.6 ± 12.6	***0.0285***
Adaptation ratio (ISI_3/ISI_9)	0.86 ± 0.22	1.00 ± 0.30	0.3587

Italic bold font indicates significant differences; *$p < 0.05$, **$p < 0.01$, ***$p < 0.001$ for Wilcoxon Mann–Whitney *U* test. Data were collected from $n = 51$ rats.

$n = 13$ neurons). Untufted PNs had apical dendrites ending in either L1 or L2, but only a small proportion of the total apical dendritic length was in the terminating layer. Apical dendrites of the PNs in this sub-cluster often formed apical oblique dendrites in L3 and L5 accounting for more than 70% of the total length. Apical dendrites of short PNs terminated in L5 or L6; in general, dendrites were almost exclusively restricted to deep layers (Fig. 1C,D).

Apart from the classical "upright" excitatory neurons, there were also 31 inverted/horizontally oriented neurons including 5 bipolar inverted neurons and 26 inverted excitatory neurons. Unlike the normal bipolar neurons in cluster 1, the inverted bipolar neurons were diverse in terms of their longest secondary dendrites, but all have primary leading dendrites projecting toward the white matter. In the sub-cluster of inverted excitatory neurons, neurons have only one major dendrite projecting either

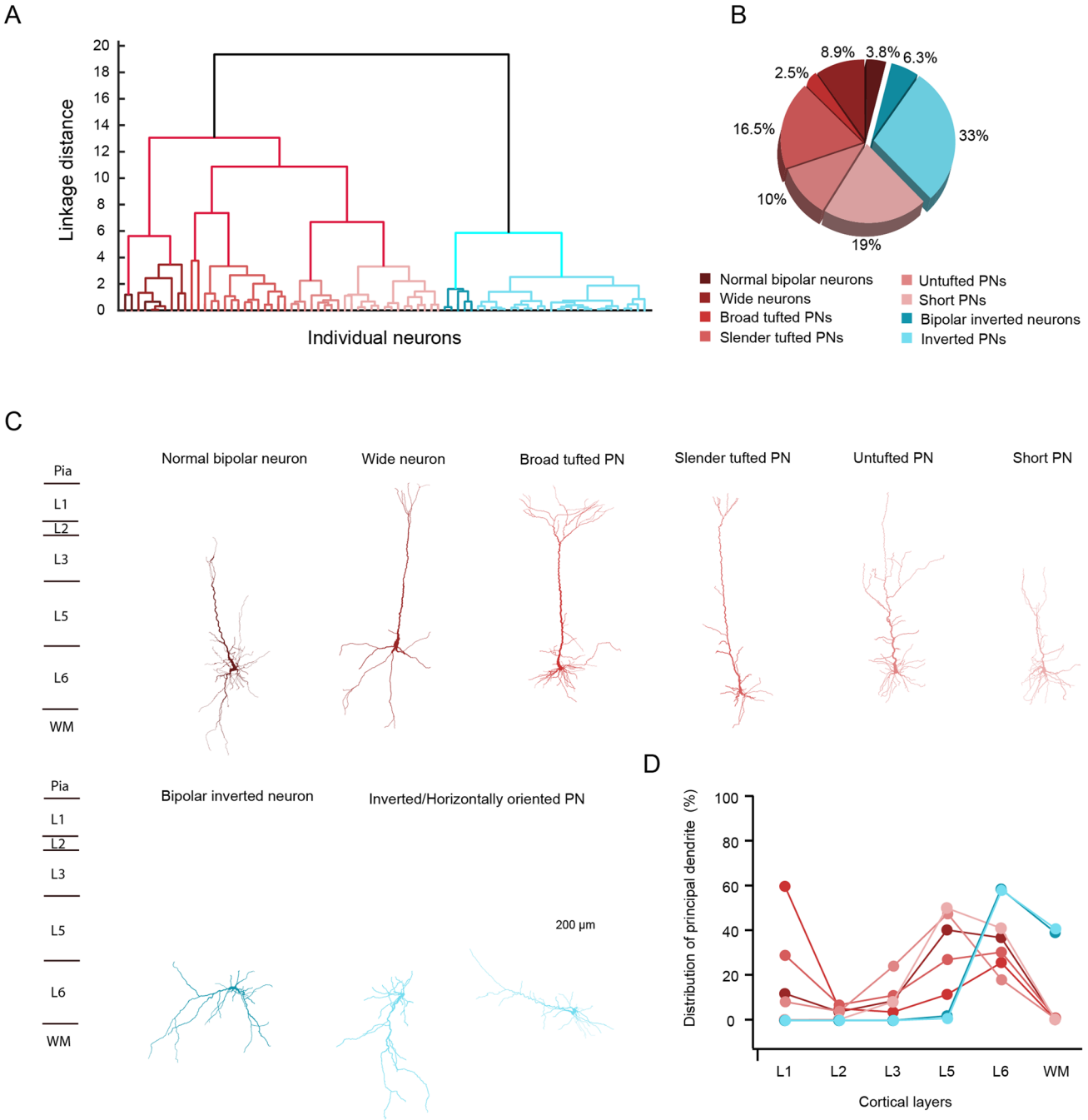


Figure 1. Identification of two distinct morphological types of L6 excitatory neurons in rat mPFC using cluster analysis. ***A***, Dendrogram from cluster analysis of morphological parameters reveals 2 main clusters and 8 distinct sub-clusters ($n = 79$ neurons from 51 rats). The *X*-axis shows individual neurons and the *Y*-axis corresponds to the linkage distance measured by Euclidean distance. Cluster 1 and Cluster 2 are represented by a spectrum of colors ranging from red to blue. ***B***, Pie chart showing the percentage of each sub-cluster, with corresponding sub-cluster colors aligning with those in panel (***A***). ***C***, Examples of dendritic morphology from the 8 sub-clusters of L6 excitatory neurons. ***D***, The proportion of the apical dendrite extending through L1–6, and the white matter (WM) is indicated by filled dots. Each dot represents the average value derived from all neurons within the respective sub-cluster. The color code used for the different L6 excitatory sub-clusters in panels ***A,B*** also applies to panels ***C,D***.

toward and often into the WM or horizontally to it. All neurons in cluster 2 have main dendrites restricted to L6 and WM (Fig. 1 *C,D*). Notably, the leading dendrites of L6 inverted neurons are longer than those of upright neurons (3,621 ± 946 vs 3,098 ± 1,439 µm, $*p < 0.05$), but the total length of basal dendrites is shorter (1,625 ± 590 vs 2,413 ± 1,085 µm, $***p < 0.001$).

Upright and inverted excitatory neurons show distinct electrophysiological properties

To determine whether neurons belonging to either of the two morphological clusters identified here have different electrophysiological properties, their passive membrane properties, single AP properties and firing behavior were analyzed. Neurons with a resting membrane potential less negative than −55 mV or a series resistance higher than 40 MΩ were excluded from the final data set. Therefore, electrophysiological parameters from 20 upright neurons and 11 inverted neurons were used for statistical comparison.

L6 upright and inverted excitatory neurons show significant differences in their passive and active electrophysiological properties. Inverted excitatory neurons had a more depolarized mean resting membrane potential (−60.55 ± 4.03 vs −66.8 ± 5.18 mV, $**p < 0.01$) when compared to upright excitatory neurons. Although the input resistance (R_{in}) of neurons in both clusters was higher than that of neurons in other layers (van Aerde and Feldmeyer, 2015), it was exceptionally high in inverted excitatory neurons, whose R_{in} was almost twice that of upright excitatory neurons, (396.08 ± 95.97 vs 235.93 ± 77.26 MΩ, $***p < 0.001$), resulting in a slower membrane time constant (34.27 ± 7.46 vs 25.35 ± 5.66 ms, $p < 0.001$) for inverted neurons (Fig. 2*A*). This indicates that the two L6 neuron clusters differed significantly in their excitability. Consistent with this, upright neurons were significantly less excitable than inverted neurons as indicated by rheobase values of 112.5 ± 39.32 and 49.09 ± 13 pA, respectively ($***p < 0.001$). Furthermore, upright excitatory neurons showed a more hyperpolarized AP threshold compared to inverted neurons (−29.46 ± 3.16 vs −33.21 ± 4.54 mV, $*p < 0.05$; Fig. 2*C*). The 3D scatter plot in Figure 2*B* shows that excitatory neurons in layer 6 of the mPFC can be reliably distinguished by both morphological and physiological features.

In addition, the AP half-width was much shorter in L6 upright excitatory neurons than in inverted excitatory neurons (1.34 ± 0.16 vs 1.06 ± 0.14 ms, $***p < 0.001$), as expected from the higher capacitive load (i.e., high R_m and slow τ_m) in the latter. Most L6 excitatory neurons in the mPFC had a regular firing pattern; however, some of these regular spiking neurons displayed a very short first interspike interval (ISI) at the beginning of the spike train. As this affects the second ISI, the adaptation ratios were measured as the ratio of third and ninth ISI (ISI_3/ISI_9) for all excitatory neurons. There was no major difference in AP firing adaptation of both upright and inverted excitatory neurons. Using current injections of the same amplitude, inverted excitatory neurons fired more APs, resulting in a significantly smaller mean ISI value than upright excitatory neurons (78.63 ± 12.6 vs 90.19 ± 12.78 ms, $*p < 0.05$) (Fig. 2*D*). Further electrophysiological properties and the statistical comparison of the two excitatory L6 neuron types are shown in Table 1.

It has been reported that adenosine-mediated modulation of synaptic transmission and plasticity displays an ontogenic variation (Descombes et al., 1998; Costenla et al., 2011). To investigate the variation of neuronal characteristics in the two distinct groups during postnatal development, we conducted whole-cell recordings from L6 excitatory neurons in rats aged between 4 weeks and 2 months. Among 18 recorded neurons, 12 are upright and 6 are inverted excitatory neurons, reflecting a ratio of 67–33%, which is similar to our findings of two morphological groups in juvenile rats (61–39%). Electrophysiological properties were compared between upright and inverted neurons. Consistent with our findings in juvenile rats, inverted neurons exhibited higher input resistance, a smaller rheobase current, a more depolarized action potential (AP) threshold, and a broader AP half-width (Fig. 2*E,F*). These observations suggest that the differences in electrophysiological properties between upright and inverted excitatory neurons persist from preadolescence into young adulthood.

Upright and inverted neurons form synaptic connections with distinct functional and structural properties

Due to the low excitatory synaptic connectivity ratio in layer 6, a so-called "loose seal" search protocol (see Materials and Methods) was used to test for potential synaptic connections. A total of 159 neurons were recorded as postsynaptic neurons. Out of 1,450 potential presynaptic neurons, 45 neurons were found to be connected to the recorded postsynaptic neurons, i.e., the connectivity ratio was 3.1% in layer 6 of the mPFC. After re-patching, 20 excitatory monosynaptic connections were recorded in dual whole-cell mode. In 15 out of 20 pairs the pre- and postsynaptic neurons were morphologically reconstructed and classified according to their dendritic morphology as described in Figure 1. We identified seven synaptically coupled pairs with a presynaptic upright neuron and eight pairs with a presynaptic inverted excitatory neuron. All presynaptic upright neurons were synaptically coupled to another postsynaptic upright excitatory neuron whereas inverted neurons formed connections with either an upright ($n = 3$) or an inverted ($n = 5$) neuron.

The mean intersoma distance was found to be significantly shorter in synaptic connections between two upright excitatory neurons compared to those with a presynaptic inverted neuron (61.4 ± 33.0 vs 107.7 ± 32.0, $*p < 0.05$) (Fig. 3*A*). The E→E connections with a presynaptic upright excitatory neurons displayed unitary EPSPs (uEPSPs) with an average amplitude of 0.22 ± 0.23 mV, which is significantly smaller than that evoked by presynaptic inverted excitatory neurons (1.03 ± 0.61 mV, $*p < 0.05$). Most pairs (6 out of 7) with a presynaptic upright excitatory neuron showed strong short-term facilitation resulting in an average paired-pulse ratio (PPR) of 3.6 ± 3.9. In contrast, connections established by inverted excitatory neurons all showed short-term depression, characterized by a mean PPR of 0.68 ± 0.14 (Fig. 3*B*).

It has been reported that inverted pyramidal neurons have long and dense axonal projections in deep neocortical layers, thereby contributing to a network of long-range intracortical connections between different cortical areas (Zhang and Deschênes, 1997; Egger et al., 2020). To investigate whether the different synaptic properties depend on the distinct axonal morphology of these two L6 neuron types, we reconstructed the axons of L5 neurons in each morphology cluster. We found that the length of axon located in layer 6 was found to be significantly smaller for upright excitatory neurons than inverted excitatory neurons (2,239 ± 1,319 vs 4,553 ± 2,463 µm, $**p < 0.01$). Furthermore, the absolute horizontal axonal field span in layer 6 of upright L6 excitatory neurons was significantly smaller than that of inverted L6 excitatory neurons (491 ± 273 vs 906 ± 492 µm, $**p < 0.01$). The ratio between the horizontal and vertical axonal field span was also significantly different between upright and inverted excitatory neurons (0.92 ± 0.42 and 1.56 ± 0.81, respectively; $*p < 0.05$), indicating that inverted excitatory neurons have a prominent axonal projections

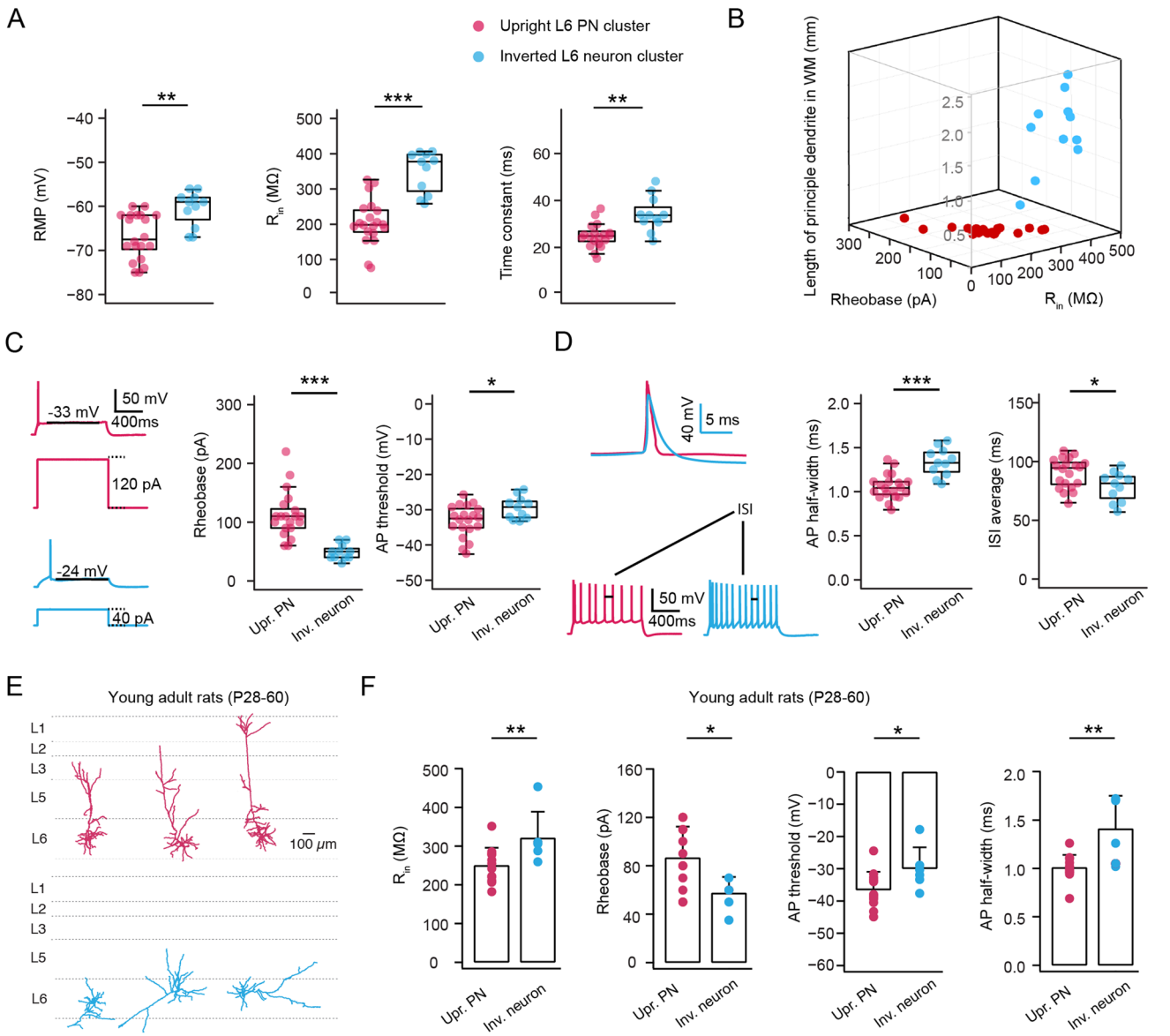


Figure 2. Upright and inverted L6 excitatory neurons show distinct electrophysiological properties. ***A***, Difference in resting membrane potential (RMP), input resistance (R_{in}) and membrane time constant in upright L6 excitatory neurons ($n = 20$ neurons, red) and inverted L6 excitatory neurons ($n = 11$ neurons, cyan). $^{**}p < 0.01$, $^{***}p < 0.001$ for the Wilcoxon Mann–Whitney *U* test. Data were obtained from 27 rats. ***B***, The 3D scatter plot shows a clear separation of two L6 excitatory neuron clusters using morphological and electrophysiological properties. Upright L6 excitatory neurons are shown in red and inverted L6 excitatory neurons in cyan. ***C***, Difference in rheobase and AP threshold in upright L6 excitatory neurons and inverted L6 excitatory neurons. Examples are shown in the left. $^{*}p < 0.05$, $^{***}p < 0.001$ for the Wilcoxon Mann–Whitney *U* test. ***D***, Difference in AP half-width and mean interspike interval (ISI) in upright L6 excitatory neurons and inverted L6 excitatory neurons. Examples are shown on the left. $^{*}p < 0.05$, $^{***}p < 0.001$ for the Wilcoxon Mann–Whitney *U* test. ***E***, Representative morphological reconstructions of L6 upright (top) and inverted (bottom) excitatory neurons recorded in mPFC of young adult rats (P28–P60). ***F***, Summary data of several electrophysiological properties of L6 upright ($n = 12$ neurons) and inverted ($n = 6$ neurons) excitatory neurons in mPFC of young adult rats (data from 8 rats).

along the horizontal axis (Fig. 3*C*,*D*). It should be noted that for inverted neurons, this ratio is severely underestimated due to the high degree of truncation of long-range axonal collaterals during acute brain slice preparation. Taken together, our results demonstrate a strong correlation between presynaptic neuronal morphology and postsynaptic uEPSP properties.

The neuromodulator adenosine reduces presynaptic neurotransmitter release in L6 excitatory neurons via activating A_1ARs

To elucidate the adenosinergic modulation of excitatory synaptic transmission, paired recordings were performed from synaptically coupled mPFC L6 neurons (Fig. 4*A*). We found that adenosine strongly suppressed the synaptic efficacy of all the L6 excitatory connections without exception (Fig. 4*B–D*). For L6 excitatory connections, the postsynaptic mean uEPSP amplitude decreased from 0.75 ± 0.67 to 0.14 ± 0.15 mV ($n = 15$ connections, $^{***}p < 0.001$) while the PPR increased from 1.12 ± 0.80 to 2.42 ± 2.45 ($^{***}p < 0.001$) after bath application of 30 μM adenosine. In addition, the CV increased from 0.82 ± 0.47 to 1.29 ± 0.33 ($^{**}p < 0.01$) and the failure rate increased from $31.9 \pm 31.4\%$ to $72.3 \pm 16.2\%$ ($^{***}p < 0.001$) at these connections (Fig. 4*D*). No significant changes in EPSP latency, 20–80% rise time and decay time were found, suggesting that adenosine suppresses synaptic transmission of excitatory connections predominantly via a presynaptic mechanism (Table 2). To investigate whether adenosine inhibits

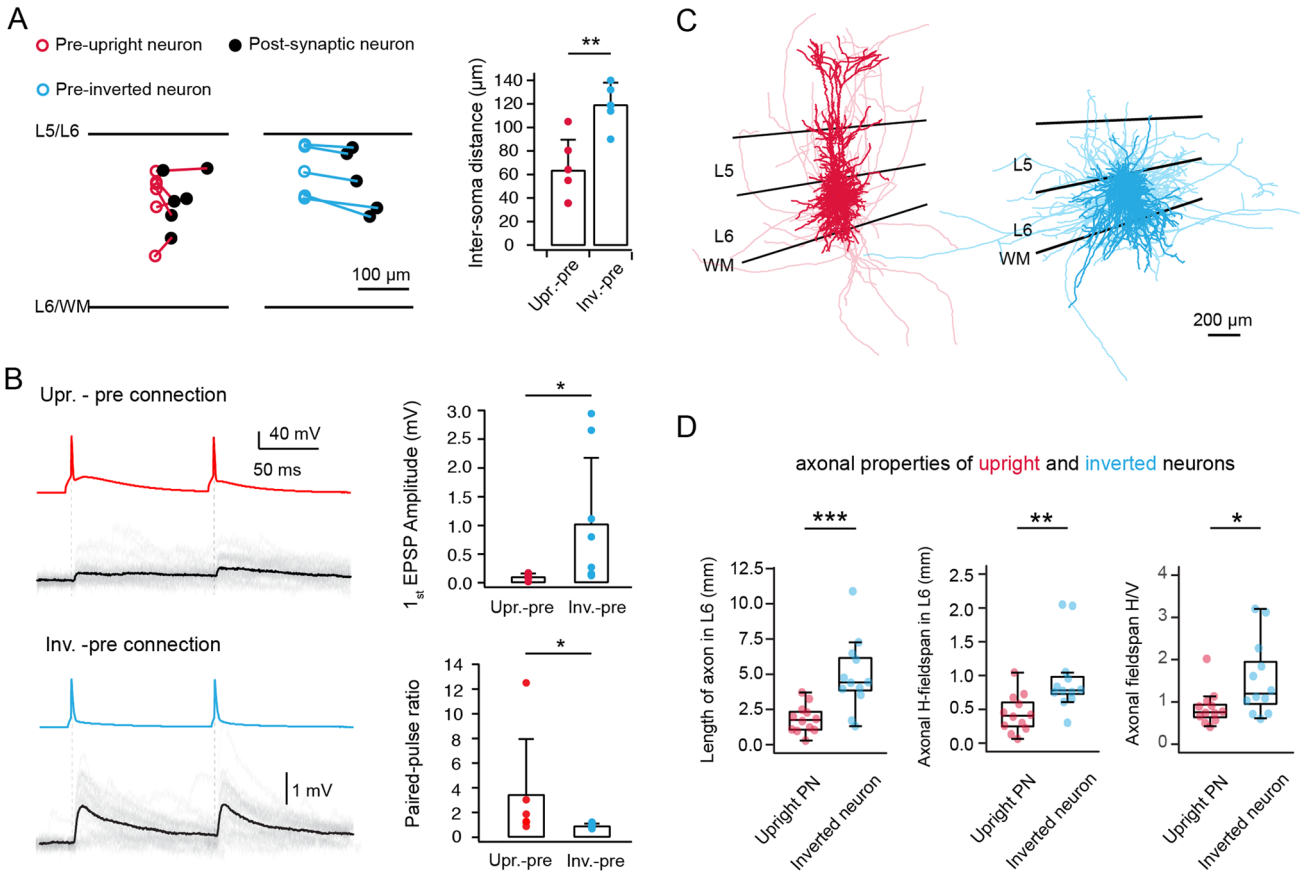


Figure 3. Functional properties of L6 E→E connections depend on the different presynaptic neuron subtypes. ***A***, Left, the position in layer 6 and intersoma distance of pre- and postsynaptic neurons in each pair are shown. Presynaptic neurons are color-coded in red and cyan for upright and inverted neurons, respectively; postsynaptic neurons are shown in black. The plot was constructed by aligning the L5/L6 borders. Right, Histogram comparing the intersoma distance for connections with a presynaptic upright and presynaptic inverted L6 neuron, respectively. $^{**}p < 0.01$ for the Wilcoxon Mann–Whitney *U* test. ***B***, Left, unitary synaptic connections in mPFC layer 6 with a presynaptic upright (top) or inverted (bottom) excitatory neuron. EPSPs are elicited by two presynaptic APs at an interstimulus interval of 100 ms. The mean uEPSP waveform is shown in black and the individual sweeps are shown in light gray. Right, histograms showing differences in first uEPSP amplitude and paired pulse ratio between upright- ($n = 7$) and inverted-pre ($n = 8$) connections. $^{**}p < 0.05$ for the Wilcoxon Mann–Whitney *U* test (data from 15 rats). ***C***, Superimposed morphological reconstructions of upright (red, $n = 15$) and inverted (cyan, $n = 15$) neurons. The somatodendritic domain is shown in a darker, the axons in a lighter shades. Layer borders of L3/L5, L5/L6 and L6/WM are indicated by black lines from top to bottom (data from 17 rats). ***D***, Summary data of several axonal properties of L6 upright ($n = 12$) and inverted ($n = 12$) excitatory neurons in rat mPFC (data from 14 rats).

presynaptic release in a cell type-dependent manner, presynaptic neurons were classified either as upright or inverted neurons based on the above criteria. We found that bath application of 30 μM adenosine reduced the amplitude of uEPSP at connections with a presynaptic upright neuron to 27 ± 16% of control, and at connections with a presynaptic upright excitatory neuron the uEPSP amplitude was reduced to 25 ± 21% of control. Thus, following the application of 30 μM adenosine, no significant change in the percentage of EPSP amplitude reduction was found between these two types of excitatory connections (Fig. 4*D*).

The inhibitory effects of adenosine on synaptic transmission via A_1ARs have been extensively investigated in the hippocampus (Dunwiddie and Hoffer, 1980; Dunwiddie and Fredholm, 1989; Moore et al., 2003; Hargus et al., 2009). Previous studies have suggested that presynaptic A_1ARs are responsible for modulating excitatory synaptic transmission in upper layers of the piriform, entorhinal and somatosensory barrel cortices (Yang et al., 2007; Wang et al., 2013; Qi et al., 2017). To investigate whether the effect of adenosine on synaptic transmission in layer 6 is induced by A_1AR activation, the A_1AR antagonist CPT (1 μM) was coapplied with adenosine (30 μM) after adenosine had been applied alone. The effect of adenosine on excitatory connections was blocked and recovered from 0.21 ± 0.18 mV to 0.52 ± 0.50 mV of the control level ($n = 9$ connections, $^{*}p < 0.05$). Coapplication of adenosine and CPT also blocked the adenosine-induced changes in other EPSP properties including the CV and failure rate (Fig. 4*E*,*F*). This suggest that adenosine decreases the neurotransmitter release probability via activation of presynaptic A_1ARs.

In L2/3 of rat visual cortex, A_{2A}ARs have no direct effect on synaptic transmission, but can modulate its A_1AR-mediated suppression (Bannon et al., 2014; Zhang et al., 2015). In L5 of rat mPFC, A_{2A}R modulate long-term plasticity at excitatory synapses onto fast-spiking interneurons rather than synaptic transmission between glutamatergic neurons (Kerkhofs et al., 2018). To elucidate whether A_{2A}ARs also participate in the adenosine-induced effects on synaptic transmission in L6 of mPFC, 30 nM of the specific A_{2A}AR agonist CGS21680 was bath-applied during recordings of excitatory connections. Synaptic properties correlated with neurotransmitter release probability were not altered by CGS21680 at L6 excitatory connections (Fig. 4*G*–*I*). Single cell recordings showed no change in the postsynaptic resting membrane potential following bath application of CGS21680 suggesting that the functional A_{2A}AR presence in mPFC L6 excitatory neurons is low at least at the soma.

To further test the presynaptic effect of adenosine, miniature spontaneous postsynaptic activity of L6 excitatory neurons was

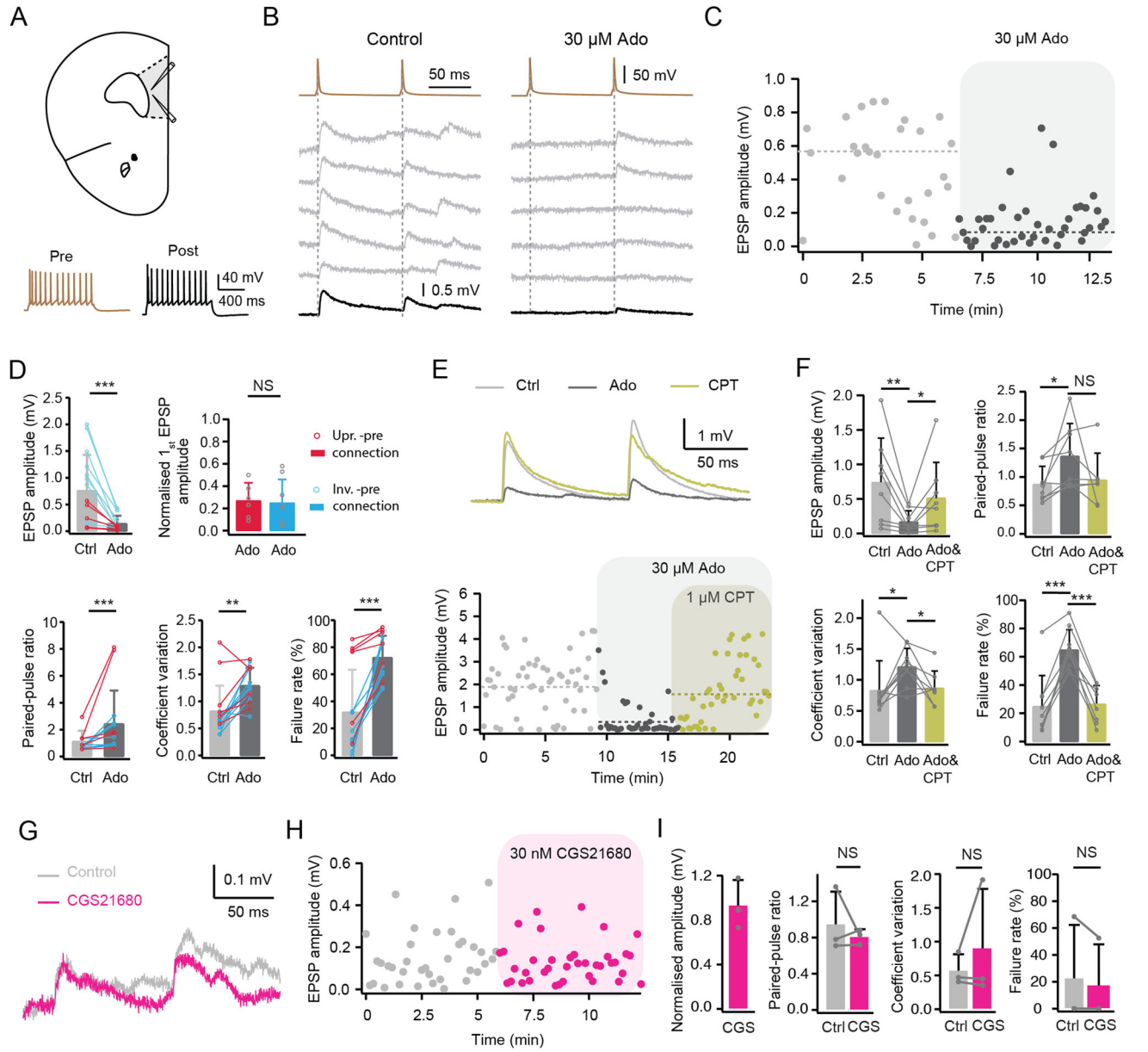


Figure 4. Adenosine suppresses presynaptic release probability of excitatory connections in layer 6 of the mPFC via A_1ARs. ***A***, Top, schematic representation of a mPFC slice with the position of the paired-recording electrodes. Bottom, pre- and postsynaptic firing patterns are shown in in brown and black, respectively. ***B***, Current clamp recordings of unitary synaptic connections in layer 6 of rat mPFC. Five consecutive uEPSPs (middle, light gray) and the average EPSP (bottom, black) are elicited by two presynaptic APs at 10 Hz (top, brown). ***C***, Time course of EPSP amplitude change following bath application of 30 μM adenosine to a L6 excitatory connection. Dashed lines indicate the mean first EPSP amplitude under control and adenosine conditions. ***D***, Summary data of several EPSP properties for L6 excitatory connections are shown. Error bars represent SD. NS (not significant), $^{**}p < 0.01$, $^{***}p < 0.001$ for Wilcoxon signed-rank test. $n = 15$ pairs from 15 rats. ***E***, Top, superimposition of EPSPs recorded in control, the presence of Ado (30 μM), and of Ado and CPT (1 μM) from a representative excitatory connection in layer 6 of rat mPFC. Bottom, time course of EPSP amplitude changes following bath application of 30 μM adenosine (ADO) and of adenosine and CPT (ADO&CPT) in the same excitatory pair. ***F***, Histograms ($n = 9$ pairs from 9 rats) showing the effect of adenosine (ADO) and CPT blockade of adenosine-induced changes (ADO&CPT) on several EPSP properties including EPSP amplitude, PPR, CV, and failure rate. Error bars represent SD. $^{*}p < 0.05$, $^{**}p < 0.01$, $^{***}p < 0.001$ for Wilcoxon signed-rank test. ***G***, Superimposition of EPSPs recorded in control and the presence of CGS21680 (30 nM) from a representative excitatory connection in layer 6 of rat mPFC. ***H***, Time course of EPSP amplitude change during application of CGS21680. ***I***, Summary data of CGS21680-induced changes in EPSP properties ($n = 3$ pairs from 3 rats). NS, not significant for paired *t* test.

recorded in voltage-clamp mode. In the presence of 0.5 μM TTX and 10 μM gabazine in the bath, miniature excitatory postsynaptic currents (mEPSCs) were recorded under control conditions and in the presence of adenosine (Fig. 5*A*). Bath application of 30 μM adenosine significantly reduced the frequency of mEPSCs from 1.0 ± 0.5 to 0.6 ± 0.4 Hz ($n = 12$ neurons, $^{***}p <$ 0.001), suggesting that an AP-independent mechanism is also involved in adenosine-induced inhibition of glutamatergic transmission. No significant change in the mEPSC amplitude was observed (10.9 ± 2.1 pA for control vs 10.8 ± 2.8 pA for adenosine) (Fig. 5*B,C*). Co-application of adenosine and CPT completely blocked the adenosine-induced decrease of the mEPSCs frequency (0.99 ± 0.52 for control vs 0.90 ± 0.43 for adenosine & CPT, $n = 15$ neurons, $p = 0.43$), indicating that decrease in mEPSC frequency in mPFC L6 excitatory neurons is mediated by A_1ARs activation (Fig. 5*D,E*). To reveal the effect of endogenous adenosine on L6 neurons, CPT was applied in the absence of adenosine. CPT significantly increased the

Table 2. uEPSP properties of L6 upright- and inverted-preconnections under control and adenosine conditions

	Ctrl	Adenosine 30 μM	Wilcoxon signed-rank test	Ctrl	Adenosine 10 μM	Wilcoxon signed-rank test
Upright-pre connections ($n = 8$ connections from 8 rats)						
1st EPSP amplitude (mV)	0.25 ± 0.23	0.05 ± 0.04	***0.0313***	0.24 ± 0.27	0.04 ± 0.04	***0.0156***
Normalized 1st EPSP amplitude (%)	-	27 ± 16	-	-	19 ± 4	-
Paired-pulse ratio	1.67 ± 1.04	4.05 ± 3.65	***0.0313***	1.20 ± 0.62	2.41 ± 2.58	0.1094
Coefficient of variation	1.14 ± 0.61	1.34 ± 0.39	0.3125	1.06 ± 0.30	1.25 ± 0.37	0.5781
Failure rate (%)	58.7 ± 33.3	80.6 ± 16.2	***0.0313***	59.1 ± 17.0	83.4 ± 4.0	***0.0313***
Rise time (ms)	0.91 ± 0.22	1.25 ± 0.30	0.2188	1.13 ± 0.28	0.71 ± 0.19	0.7656
Latency (ms)	1.55 ± 0.63	1.56 ± 0.80	0.5781	1.46 ± 0.60	1.31 ± 0.70	0.5625
Decay time (ms)	28.5 ± 29.8	27.4 ± 27.1	0.8438	22.2 ± 14.5	23.7 ± 19.3	0.5781
Inverted-pre connections ($n = 8$ connections from 8 rats)						
1st EPSP amplitude (mV)	0.99 ± 0.62	0.17 ± 0.15	****0.0078***	1.20 ± 0.89	0.68 ± 0.52	***0.0156***
Normalized 1st EPSP amplitude (%)	-	25 ± 21	-	-	58 ± 19	-
Paired-pulse ratio	0.67 ± 0.13	1.54 ± 0.93	***0.0156***	0.89 ± 0.32	0.89 ± 0.23	0.8906
Coefficient of variation	0.60 ± 0.16	1.21 ± 0.29	****0.0078***	0.70 ± 0.27	0.89 ± 0.26	0.0781
Failure rate (%)	13.6 ± 12.2	68.9 ± 13.9	****0.0039***	25.2 ± 21.8	38.1 ± 20.7	***0.0469***
Rise time (ms)	1.44 ± 0.74	1.31 ± 0.87	0.5469	1.56 ± 0.73	1.32 ± 0.79	0.1719
Latency (ms)	1.32 ± 0.47	1.24 ± 0.67	0.6406	1.38 ± 0.45	1.89 ± 1.02	0.1563
Decay time (ms)	46.6 ± 25.8	46.1 ± 42.8	0.5273	40.5 ± 15.7	35.9 ± 38.0	0.6875

Bold italic font indicates significant differences to control; $*p < 0.05$, $**p < 0.01$ for Wilcoxon signed-rank test.

miniature excitatory postsynaptic current (mEPSC) frequency in L6 neurons from 0.99 ± 0.52 to 1.20 ± 0.65 Hz (Fig. 5*F,G*, indicating that endogenous adenosine exerts an inhibitory effect on presynaptic inputs on L6 excitatory neurons). Comparison of the relative proportion of this increase between the two neuronal clusters did not yield any statistically significant differences.

Connections with a presynaptic upright excitatory neuron are more sensitive to low concentration of adenosine

In the PFC, the concentration of endogenous adenosine release ranges widely from nanomolar to micromolar concentration (Fredholm, 2007; Nguyen et al., 2014). In layer 4 of the barrel cortex, adenosine suppresses excitatory synaptic transmission with a half-maximal effective concentration of 9.6 μM (Qi et al., 2017). Here, we used a lower concentration of adenosine (10 μM) to test whether presynaptic upright and inverted neurons show differential sensitivity to adenosine. Although the connections established by an inverted excitatory neuron and an upright excitatory neuron showed no significant difference in their response to 30 μM adenosine, we found that connections established by L6 upright excitatory neurons are more sensitive to a lower concentration of adenosine. Bath application of 10 μM adenosine decreased the uEPSP amplitude at connections with a presynaptic upright excitatory neuron to 19 ± 4% of control (Fig. 6*A,C,D*). In contrast, the uEPSP amplitude at connections with a presynaptic inverted excitatory neuron was reduced to only 58 ± 19% of control after applying the same adenosine concentration (Fig. 6*B,E,F*). This was significantly higher compared to the connections established by an upright excitatory neurons ($n = 8$ for each connection type, $***p < 0.001$, Fig. 6*G*, Table 2). More details of the functional properties of two connection types under control and 10 μM adenosine conditions are shown in Table 2.

To test whether the difference in adenosine sensitivity was mediated by postsynaptic adenosine receptors, the postsynaptic membrane potential was measured simultaneously following bath application of 10 μM adenosine. No significant difference in the amplitude of adenosine-induced hyperpolarization was found between the two types of L6 excitatory neuron (Fig. 6*H*). These findings suggest that the presynaptic release sites of upright excitatory neurons have a greater sensitivity to low concentration of adenosine compared to those of inverted excitatory neurons. Nevertheless, the change in membrane potential is predominantly mediated by receptors located at the soma; therefore it is possible that the two neuron types also differ in their adenosine sensitivity at the postsynaptic dendritic sites.

Discussion

Layer 6 of the mPFC remains a largely unexplored brain region with a highly heterogeneous cellular composition. Here we classified excitatory neurons in mPFC layer 6 into two main morphological groups based on their dendritic arborization pattern: upright pyramidal cell-like and inverted neurons. We found that (1) upright and inverted excitatory neurons have different electrophysiological properties with the latter having a higher intrinsic excitability. (2) Upright excitatory neurons establish weak, facilitating synapses with other L6 neurons whereas synapses formed by inverted cells show a higher EPSP amplitude and a pronounced short-term depression. This may be due to the distinct axonal projecting pattern of these two L6 neuron types within their home layer. In addition, (3) adenosine induced a reduction of the neurotransmitter release probability in L6 excitatory neurons via activation of presynaptic A_1ARs. Although 30 μM adenosine strongly suppressed connections with both presynaptic upright or inverted excitatory neurons, (4) synapses formed by L6 upright neurons are more sensitive to low concentrations of adenosine (10 μM). Our results reveal that two functionally and morphologically distinct subpopulations of L6 principal neurons are differentially affected by adenosine, suggesting that they may play distinct roles in the maintenance of sleep homoeostasis by adenosine.

Upright and inverted projection neurons in layer 6 of mPFC

L6 excitatory neurons show a high degree of morphological diversity in all neocortical areas including the mPFC (Yang et al., 1996, 2022; Zhang and Deschênes, 1997; Kumar and Ohana, 2008; Thomson, 2010; Pichon et al., 2012; Marx and Feldmeyer, 2013; van Aerde and Feldmeyer, 2015). In the

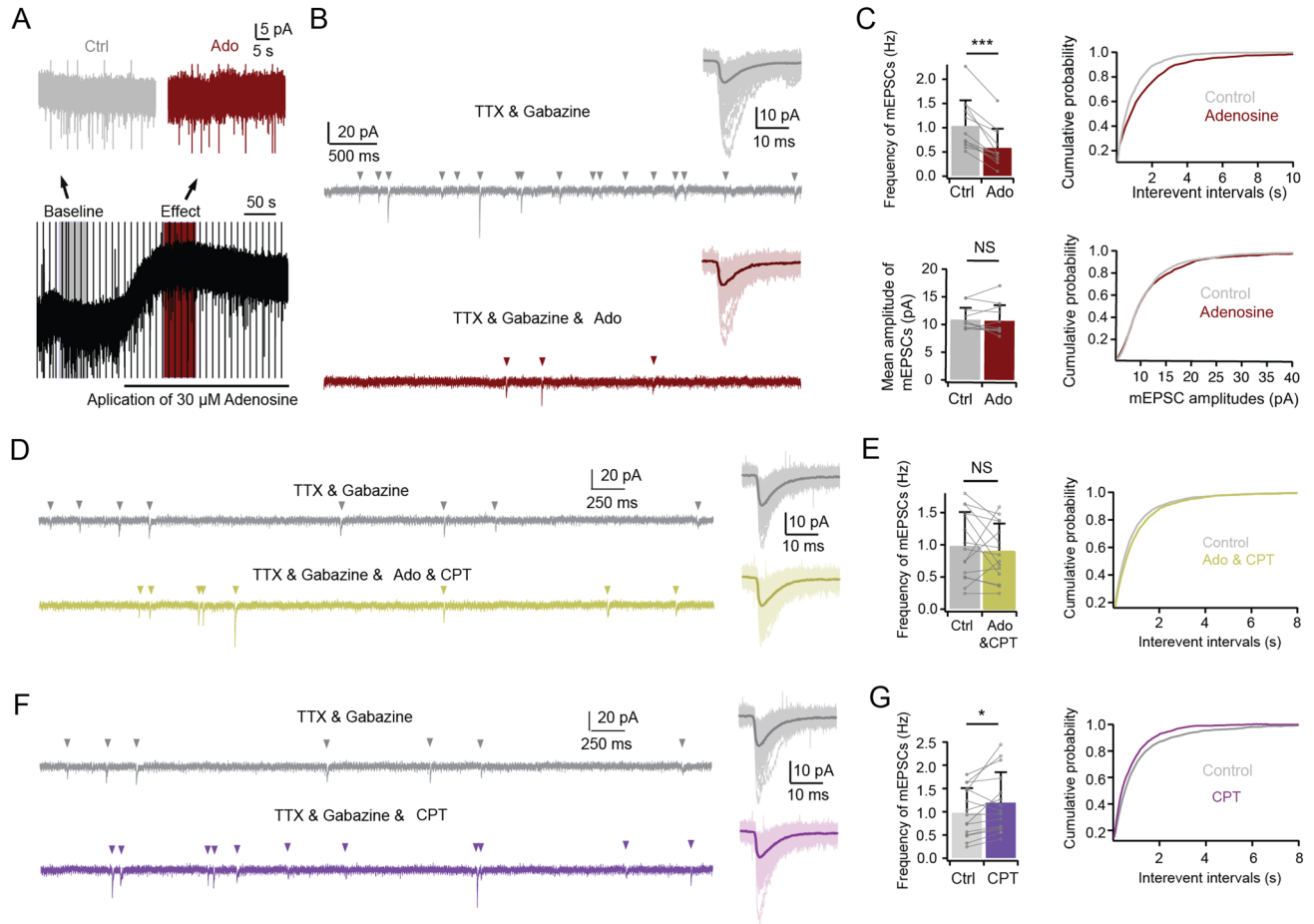


Figure 5. Modulation of miniature spontaneous synaptic activity in L6 excitatory neurons by adenosine through A_1 receptor activation. ***A***, Representative voltage-clamp recording illustrating spontaneous activity during application of TTX (0.5 μM), gabazine (10 μM), and adenosine (30 μM). ***B***, Comparison of 5 s recording epochs under control (gray) and norepinephrine (NE) conditions (dark red). Insets show overlay of miniature excitatory postsynaptic currents (mEPSCs) extracted from a 50 s continuous recording depicted in panel (***A***). The average and individual EPSCs are superimposed and given in a darker and lighter shade, respectively. ***C***, Adenosine application (30 μM) led to an increase in the interevent interval (IEI, right, 1,114 samples for control and 626 samples for adenosine from 12 cells) and a decrease in the frequency of miniature excitatory postsynaptic currents (mEPSCs), without significant alteration in mEPSC amplitudes ($n = 7$ for upright and $n = 5$ for inverted neurons; data from 5 rats). NS (not significant), $***p < 0.001$ for Wilcoxon signed-rank test. Error bars represent SD. ***D***, Comparative 5 s recording epochs under control (gray) and coapplication of adenosine (30 μM) and 8-cyclopentyltheophylline (CPT, 1 μM) conditions (light green). Insets display overlay of mEPSCs extracted from 50 s continuous recordings under control and pharmacological conditions. The average and individual mEPSCs are superimposed and given in a darker and lighter shade, respectively. ***E***, Coapplication of adenosine (30 μM) and CPT (1 μM) restored adenosine-induced reduction in mEPSC frequency to control levels ($n = 15$ neurons; data from 7 rats). NS (not significant) for Wilcoxon signed-rank test. Error bars represent SD. ***F***, Comparative 5 s recordings under control (gray) and application of CPT (1 μM) conditions (purple). Insets display overlay of mEPSCs extracted from 50 s continuous recordings under control and pharmacological conditions. The average and individual EPSCs are superimposed and given in a darker and lighter shade, respectively. ***G***, Application of CPT alone slightly increased mEPSC frequency in both upright ($n = 11$) and inverted excitatory neurons ($n = 6$; data from 7 rats). NS (not significant), $*p < 0.05$ for Wilcoxon signed-rank test. Error bars represent SD.

neocortex the incidence of inverted excitatory neurons is as low as 1% of rat (Parnavelas et al., 1977) and this fraction varies through species and brain area (up to 8.5%) (Globus and Scheibel, 1967; Qi et al., 1999; Mendizabal-Zubiaga et al., 2007). They are most numerous in deep layers in all studied species (Mendizabal-Zubiaga et al., 2007). In rat barrel cortex the percentage of inverted neurons among all excitatory neurons in layer 6A was only 2.6% (Yang et al., 2022) but was found to be up to 10% in layer 6B (Marx and Feldmeyer, 2013). Due to the small proportion of inverted spiny cells in the total principal cell population, their electrophysiological and functional properties have not been systematically investigated. It is worth noting that inverted excitatory neurons were found in abundance in reeler mutant mice which are characterized by an aberrant cortical layer formation due to reelin deficiency during the corticogenesis (Landrieu and Goffinet, 1981; Forster, 2014). In this study, we conducted an unsupervised CA based on neuronal dendritic morphology. This approach allowed for an objective and quantitative classification of mPFC L6 excitatory neurons, grouping them into distinct categories based on their leading dendritic orientation: upright or inverted/horizontally oriented neurons. Our findings revealed that nonpyramidal neurons constituted a substantial portion, accounting for 39% of the total principal neuron populations. Even when excluding bipolar inverted ($n = 5$) and horizontally oriented ($n = 1$) neurons, 25 typical inverted excitatory neurons remained, comprising 32% of our sample of L6 excitatory neuron. This remarkable prevalence of inverted excitatory neurons highlights their potentially crucial role within the L6 microcircuitry of the mPFC.

In addition to the distinct dendritic morphology, further differences were observed when comparing the electrophysiological properties of the two morphologically identified types of mPFC L6 excitatory neurons. Although all the excitatory neurons in layer 6 are unique with their high cellular input resistance

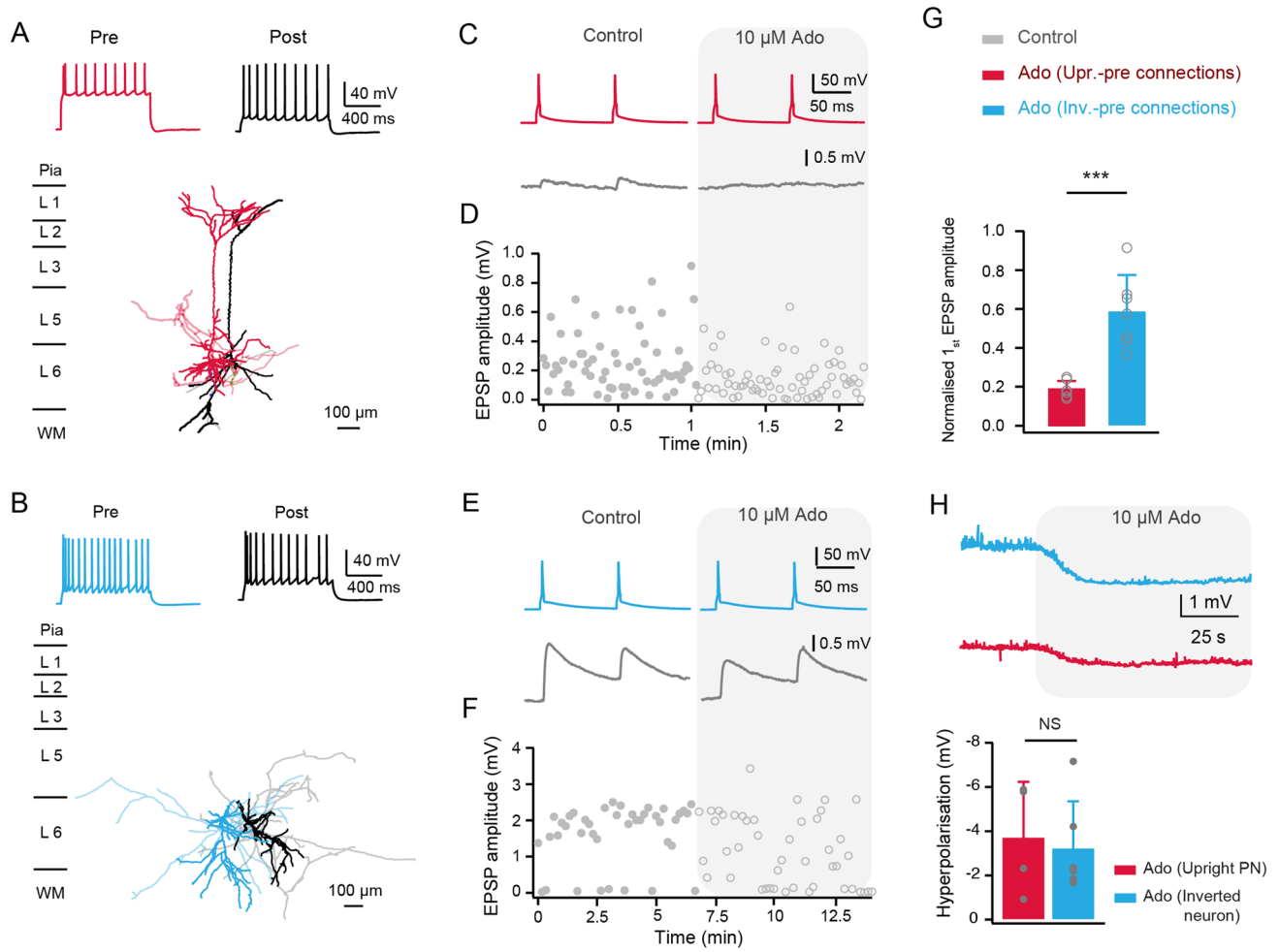


Figure 6. Excitatory connections with a presynaptic upright or inverted neuron showed different sensitivities to adenosine. ***A,B***, Morphological reconstructions of a synaptically coupled L6 upright-upright (***A***) and inverted-inverted (***B***) pair. The presynaptic somatodendritic domain is shown in a darker red and blue for upright and inverted neurons, respectively; their axons are shown light red and blue. Postsynaptic soma and dendrites are in black, and postsynaptic axons are in gray. The corresponding firing patterns of pre- and postsynaptic neurons are shown on the top. ***C,E***, Average EPSPs recorded in control and the presence of adenosine (10 µM) from a representative connection with a presynaptic upright (***C***) and an inverted (***E***) excitatory neuron. Presynaptic APs are shown at the top. ***D,F***, Time course of EPSP amplitude changes during application of 10 µM adenosine for a connection with a presynaptic upright (***D***) and inverted (***F***) neuron. ***G***, Summary data (connections with presynaptic upright neurons, $n = 7$; connections with presynaptic inverted neurons, $n = 7$) of adenosine-induced changes in EPSP amplitude. Data were collected from 14 rats. $***p < 0.001$ for Wilcoxon Mann–Whitney *U* test, error bars represent SD. ***H***, Top, representative current-clamp recordings of a postsynaptic upright and inverted neuron following bath application of 10 µM adenosine. Bottom, Adenosine-induced (10 µM) hyperpolarization of the resting membrane potential with two neuron types (inverted excitatory neurons, $n = 6$, upright excitatory neurons, $n = 5$; data from 11 rats). NS, not significant for Wilcoxon Mann–Whitney *U* test, error bars represent SD.

resulting in a high excitability (van Aerde and Feldmeyer, 2015), inverted excitatory neurons have a more depolarized resting membrane potential and AP threshold, larger membrane input resistance and time constant, longer AP half-width, smaller rheobase when compared to upright excitatory neurons. This is in consistent with a previous study in primary somatosensory cortex, which reported that inverted excitatory neurons have different passive and active physiological properties compared to upright excitatory neurons (Steger et al., 2013). Differences between inverted and upright excitatory neurons in resting membrane potential and input resistance suggest a potential difference in the distribution of ion channels that determine intrinsic electrophysiological properties, such as the potassium leak channel (Lesage, 2003). Differential AP threshold, halfwidth, and firing frequency are probably due to differences in ion channels contributing to action potential initiation and repolarization such as voltage-gated sodium channel and potassium channel types (Miller et al., 2008). Taken together, these findings strongly indicate that inverted excitatory neurons exhibited an elevated intrinsic neuronal excitability, predisposing them to the integration of inputs at supra-threshold levels. Supporting this notion, our results revealed that inverted excitatory neurons exhibit a higher frequency of APs compared to upright neurons when subjected to equivalent levels of current injection.

In addition to the distinct morphological and electrophysiological features, we found that L6 upright and inverted neurons also display different synaptic properties when forming connections. Upright excitatory neurons established synaptic connections at a small intersoma distance, whereas that of inverted neuron connections was marked larger. This may result from their different axonal projection patterns: L6 upright excitatory neurons in mPFC send their axons to subcortical areas including the thalamus, claustrum, striatum, and lateral hypothalamus (Hoover and Vertes, 2007). For instance, L6 corticothalamic neurons invariably show an upright dendritic morphology with an apical dendrite pointing toward the pial surface (Cotel et al., 2018; Hoerder-Suabedissen et al., 2018). However, inverted excitatory neurons are known to form intratelencephalic projections

including intracortical and callosal projections (Reblet et al., 1992; Mendizabal-Zubiaga et al., 2007). Our axonal reconstructions showed that inverted excitatory neurons have prominent horizontal axonal projections compared to upright neurons, particularly within their home layer 6. Moreover, we found that upright excitatory neurons establish weak facilitating synapses, while synaptic connections made by inverted excitatory neurons display larger uEPSP amplitudes and show short-term depression. In rat primary somatosensory cortex, such weak and strong synapses were found to be established by corticothalamic and corticocortical excitatory neurons, respectively (Mercer et al., 2005; West et al., 2006; Yang et al., 2022). These dynamic properties are specific to presynaptic neuron class, but not dependent on postsynaptic target-dependent. Our findings suggest that upright and inverted excitatory neuron populations are interconnected but functionally separable, with important implications for intracortical network function and subcortical output of mPFC layer 6.

Adenosine modulation of the L6 microcircuitry in the mPFC

In layer 6 of the mPFC, adenosine induced a membrane potential hyperpolarization and suppressed synaptic transmission via post- and presynaptic A_1ARs, respectively. It has been shown that block of K_{ir} channels abolishes the adenosine-induced membrane hyperpolarization but not the inhibition of synaptic transmission in hippocampus, brainstem and neocortex (Gerber et al., 1989; Thompson et al., 1992; Rainnie et al., 1994; Qi et al., 2017). This suggests that K_{ir} channels are only involved in the postsynaptic effect of adenosine (Luscher et al., 1997; van Aerde and Feldmeyer, 2015). The inhibition of synaptic transmission by adenosine via A_1ARs is most likely due to a reduction of presynaptic neurotransmitter release resulting from a reduction in calcium influx through presynaptic voltage-dependent calcium channels (Wu and Saggau, 1994, 1997). The effect of adenosine was concentration dependent and the low EC_{50} suggests that the presynaptic release probability and hence presynaptic calcium channels are more sensitive to adenosine than K_{ir} channels (Wu and Saggau, 1994; van Aerde and Feldmeyer, 2015; Qi et al., 2017).

Cell type-specific modulatory effects of adenosine via activation of A_1ARs have been reported previously. Excitatory but not inhibitory synapses were selectively suppressed by adenosine in cortical layer 4 and in hippocampal cultures (Yoon and Rothman, 1991; Qi et al., 2017). A_1AR activation selectively inhibits $GABA_A$ receptor currents in a specific subpopulation of hippocampal interneurons expressing axonal cannabinoid receptor type 1 (Rombo et al., 2016). However, the cell type-specific effects of adenosine on morphologically identified monosynaptic connections have not been reported yet. Applying low concentrations of adenosine (here 10 μM) to distinct excitatory synaptic connections revealed a difference in the degree of adenosine-mediated suppression between connections with a presynaptic upright and inverted neurons, respectively. Connections with an upright presynaptic neuron are more sensitive to adenosine compared to those with an inverted presynaptic neuron. This may result from a difference in the density of coupled A_1ARs at the plasma level and/or a difference in calcium channel types at the presynaptic terminals of the two connection subtypes (Wu and Saggau, 1994). However, when adenosine was applied at a concentration of 30 μM, the effect on synaptic transmission was largely similar for both types of mPFC L6 excitatory neurons. This suggests that at this higher adenosine concentration all L6 excitatory connections were strongly suppressed via A_1AR activation, thereby masking the cell type-specific effect of adenosine.

Application of the A_1AR antagonist CPT alone revealed the presence of endogenous extracellular adenosine in the mPFC slice preparation. In the presence of CPT alone the membrane potential became more depolarized and the spontaneous mEPSC frequency increased through a block of the tonic adenosine effect. In rat neocortex, the endogenous adenosine was estimated to be 1–2 μM, suggesting that the tonic modulation is only small and mainly affects synaptic release (Kerr et al., 2013; Qi et al., 2017). In hippocampus CA1 synapses, Mitchell et al. (1993), first provided evidence that adenosine release is activity-dependent. A recent study in the hippocampus showed that endogenous adenosine within excitatory synapses can vary from 8 to 60 μM under basic (0.1 Hz) to high frequency (100 Hz) stimulation (Lopes et al., 2023). These values are much higher than the previously reported levels of extrasynaptic adenosine. An activity-dependent release of adenosine has also been found for rat neocortex (Wall and Richardson, 2015). Thus, the rapid activity-dependent change in the endogenous adenosine concentration, in conjunction with its cell type- and concentration-dependent regulation of neuronal excitability and synaptic transmission reported here for layer 6 of the mPFC, indicates that adenosine plays an important role in the dynamic control of different neuronal pathways.

We also analyzed the miniature spontaneous synaptic activity in L6 excitatory neurons of the mPFC. Adenosine dramatically decreased the frequency of miniature EPSCs (mEPSCs) via activation of A_1ARs, but no changes of mEPSC amplitude were observed. Synaptic inputs onto L6 excitatory neurons originate from the thalamus or from inter- and intralaminar areas. Our finding suggests that adenosine exerts its inhibitory effect via A_1ARs at the presynaptic terminals and reduces the neurotransmitter release probability in those cortical and subcortical areas (Fontanez and Porter, 2006; Kerr et al., 2013). Previous studies on A_{2A}ARs in the hippocampus have shown that activation of these receptors enhances excitatory synaptic transmission (Rebola et al., 2003; Rombo et al., 2015). A study in rat visual cortex demonstrated a modulation of inhibitory transmission via A_{2A}ARs, which requires the activation of A_1ARs (Zhang et al., 2015). However, we did not observe significant changes in either postsynaptic membrane properties or synaptic properties during application of the A_{2A}AR agonist. This suggests minimal to no functional presence of A_{2A}ARs at both pre- and postsynaptic sites in layer 6 of the mPFC.

Adenosine has long been implicated in the promotion and maintenance of sleep, influencing sleep spindles and slow oscillations during slow wave sleep (Landolt, 2008; Bjorness et al., 2009). Absence of compensatory slow wave sleep affected working memory function which relies on the prefrontal cortical circuits (Bjorness et al., 2009). Sleep spindles are generated in the thalamus and are highly sensitive to modulation by thalamocortical and corticothalamic feedback circuits (Steriade, 2000; Bonjean et al., 2011). Slow oscillations are generated in deep layers of the neocortex and propagate to other layers depending on recurrent intracortical synaptic activity (Massimini et al., 2004; Neske, 2015). Our results show that endogenous adenosine modulates the presynaptic release of upright and inverted excitatory neurons with different sensitivity. This dynamic modulation of subcortical and intracortical synaptic transmission by adenosine may be an underlying mechanism that contributes to sleep homoeostasis. Moreover, the adenosine-induced decrease in glutamatergic synaptic transmission of L6 excitatory neurons has implications for the capacity of the mPFC to sustain persistent neural activity, a critical element supporting working memory

functions (Goldman-Rakic, 1995; Romo et al., 1999; Kilpatrick et al., 2013). Notably, the higher adenosine sensitivity of L6 corticothalamic neurons in the PFC can affect executive functions, including planning, cognitive control, decision-making, and working memory. This influence is exerted through their projections to the mediodorsal thalamus, which serves as the primary anatomically prescribed thalamic counterpart of the PFC (Gabbott et al., 2005; Mitchell et al., 2007; Chakraborty et al., 2016; Bolkan et al., 2017; Ouhaz et al., 2018). Further research is necessary to uncover the cell type-specific effects of adenosine on synaptic transmission. This will help to unravel the intricate functional role of adenosine in neuronal signaling in the brain.

References

Arrigoni E, Chamberlin NL, Saper CB, McCarley RW (2006) Adenosine inhibits basal forebrain cholinergic and noncholinergic neurons in vitro. Neuroscience 140:403–413.

Arrigoni E, Rainnie DG, McCarley RW, Greene RW (2001) Adenosine-mediated presynaptic modulation of glutamatergic transmission in the laterodorsal tegmentum. J Neurosci 21:1076–1085.

Bannon NM, Zhang P, Ilin V, Chistiakova M, Volgushev M (2014) Modulation of synaptic transmission by adenosine in layer 2/3 of the rat visual cortex in vitro. Neuroscience 260:171–184.

Basheer R, Strecker RE, Thakkar MM, McCarley RW (2004) Adenosine and sleep-wake regulation. Prog Neurobiol 73:379–396.

Bjorness TE, Kelly CL, Gao T, Poffenberger V, Greene RW (2009) Control and function of the homeostatic sleep response by adenosine A1 receptors. J Neurosci 29:1267–1276.

Bolkan SS, Stujenske JM, Parnaudeau S, Spellman TJ, Rauffenbart C, Abbas AI, Harris AZ, Gordon JA, Kellendonk C (2017) Thalamic projections sustain prefrontal activity during working memory maintenance. Nat Neurosci 20:987–996.

Bonjean M, Baker T, Lemieux M, Timofeev I, Sejnowski T, Bazhenov M (2011) Corticothalamic feedback controls sleep spindle duration in vivo. J Neurosci 31:9124–9134.

Caetano L, et al. (2017) Adenosine A(2A) receptor regulation of microglia morphological remodeling-gender bias in physiology and in a model of chronic anxiety. Mol Psychiatry 22:1035–1043.

Chakraborty S, Kolling N, Walton ME, Mitchell AS (2016) Critical role for the mediodorsal thalamus in permitting rapid reward-guided updating in stochastic reward environments. Elife 5:e13588.

Ciruela F, et al. (2006) Presynaptic control of striatal glutamatergic neurotransmission by adenosine A1-A2A receptor heteromers. J Neurosci 26: 2080–2087.

Costenla AR, Diogenes MJ, Canas PM, Rodrigues RJ, Nogueira C, Maroco J, Agostinho PM, Ribeiro JA, Cunha RA, de Mendonca A (2011) Enhanced role of adenosine A(2A) receptors in the modulation of LTP in the rat hippocampus upon ageing. Eur J Neurosci 34:12–21.

Cotel F, Fletcher LN, Kalita-de Croft S, Apergis-Schoute J, Williams SR (2018) Cell class-dependent intracortical connectivity and output dynamics of layer 6 projection neurons of the rat primary visual cortex. Cereb Cortex 28:2340–2350.

Cunha RA, Ribeiro JA (2000) Adenosine A2A receptor facilitation of synaptic transmission in the CA1 area of the rat hippocampus requires protein kinase C but not protein kinase a activation. Neurosci Lett 289:127–130.

d'Alcantara P, Ledent C, Swillens S, Schiffmann SN (2001) Inactivation of adenosine A2A receptor impairs long term potentiation in the accumbens nucleus without altering basal synaptic transmission. Neuroscience 107: 455–464.

Descombes S, Avoli M, Psarropoulou C (1998) A comparison of the adenosine-mediated synaptic inhibition in the CA3 area of immature and adult rat hippocampus. Brain Res Dev Brain Res 110:51–59.

Ding C, Emmenegger V, Schaffrath K, Feldmeyer D (2021) Layer-specific inhibitory microcircuits of layer 6 interneurons in rat prefrontal cortex. Cereb Cortex 31:32–47.

Dunwiddie TV, Fredholm BB (1989) Adenosine A1 receptors inhibit adenylate cyclase activity and neurotransmitter release and hyperpolarize pyramidal neurons in rat hippocampus. J Pharmacol Exp Ther 249:31–37.

Dunwiddie TV, Hoffer BJ (1980) Adenine nucleotides and synaptic transmission in the in vitro rat hippocampus. Br J Pharmacol 69:59–68.

Dunwiddie TV, Masino SA (2001) The role and regulation of adenosine in the central nervous system. Annu Rev Neurosci 24:31–55.

Egger R, Narayanan RT, Guest JM, Bast A, Udvary D, Messore LF, Das S, de Kock CPJ, Oberlaender M (2020) Cortical output is gated by horizontally projecting neurons in the deep layers. Neuron 105:122–137.e8.

Feldmeyer D, Egger V, Lubke J, Sakmann B (1999) Reliable synaptic connections between pairs of excitatory layer 4 neurones within a single 'barrel' of developing rat somatosensory cortex. J Physiol 521:169–190.

Feldmeyer D, Radnikow G (2016) Paired recordings from synaptically coupled neurones in acute neocortical slices. In: *Advanced patch-clamp analysis for neuroscientists* (Korngreen A, ed), 113, pp 171–191. New York: Springer Science+Business Media.

Fontanez DE, Porter JT (2006) Adenosine A1 receptors decrease thalamic excitation of inhibitory and excitatory neurons in the barrel cortex. Neuroscience 137:1177–1184.

Forster E (2014) Reelin, neuronal polarity and process orientation of cortical neurons. Neuroscience 269:102–111.

Fredholm BB (2007) Adenosine, an endogenous distress signal, modulates tissue damage and repair. Cell Death Differ 14:1315–1323.

Gabbott PL, Warner TA, Jays PR, Salway P, Busby SJ (2005) Prefrontal cortex in the rat: projections to subcortical autonomic, motor, and limbic centers. J Comp Neurol 492:145–177.

Gerber U, Greene RW, Haas HL, Stevens DR (1989) Characterization of inhibition mediated by adenosine in the hippocampus of the rat in vitro. J Physiol 417:567–578.

Globus A, Scheibel AB (1967) Pattern and field in cortical structure: the rabbit. J Comp Neurol 131:155–172.

Goldman-Rakic PS (1995) Cellular basis of working memory. Neuron 14: 477–485.

Hackett TA (2018) Adenosine A(1) receptor mRNA expression by neurons and glia in the auditory forebrain. Anat Rec 301:1882–1905.

Hargus NJ, Bertram EH, Patel MK (2009) Adenosine A1 receptors presynaptically modulate excitatory synaptic input onto subiculum neurons. Brain Res 1280:60–68.

Harrison Y, Horne JA, Rothwell A (2000) Prefrontal neuropsychological effects of sleep deprivation in young adults–a model for healthy aging? Sleep 23:1067–1073.

Hoerder-Suabedissen A, et al. (2018) Subset of cortical layer 6b neurons selectively innervates higher order thalamic nuclei in mice. Cereb Cortex 28: 1882–1897.

Hoover WB, Vertes RP (2007) Anatomical analysis of afferent projections to the medial prefrontal cortex in the rat. Brain Struct Funct 212:149–179.

Katz LC (1987) Local circuitry of identified projection neurons in cat visual cortex brain slices. J Neurosci 7:1223–1249.

Kerkhofs A, Canas PM, Timmerman AJ, Heistek TS, Real JI, Xavier C, Cunha RA, Mansvelder HD, Ferreira SG (2018) Adenosine A(2A) receptors control glutamatergic synaptic plasticity in fast spiking interneurons of the prefrontal cortex. Front Pharmacol 9:133.

Kerkhofs A, Xavier AC, da Silva BS, Canas PM, Idema S, Baayen JC, Ferreira SG, Cunha RA, Mansvelder HD (2017) Caffeine controls glutamatergic synaptic transmission and pyramidal neuron excitability in human neocortex. Front Pharmacol 8:899.

Kerr MI, Wall MJ, Richardson MJ (2013) Adenosine A1 receptor activation mediates the developmental shift at layer 5 pyramidal cell synapses and is a determinant of mature synaptic strength. J Physiol 591:3371–3380.

Kilpatrick ZP, Ermentrout B, Doiron B (2013) Optimizing working memory with heterogeneity of recurrent cortical excitation. J Neurosci 33:18999–19011.

Kumar P, Ohana O (2008) Inter- and intralaminar subcircuits of excitatory and inhibitory neurons in layer 6a of the rat barrel cortex. J Neurophysiol 100:1909–1922.

Landolt HP (2008) Sleep homeostasis: a role for adenosine in humans? Biochem Pharmacol 75:2070–2079.

Landrieu P, Goffinet A (1981) Inverted pyramidal neurons and their axons in the neocortex of reeler mutant mice. Cell Tissue Res 218:293–301.

Leffa DT, et al. (2018) Adenosine A(2A) receptors in the rat prelimbic medial prefrontal cortex control delay-based cost-benefit decision making. Front Mol Neurosci 11:475.

Lesage F (2003) Pharmacology of neuronal background potassium channels. Neuropharmacology 44:1–7.

Li Z, et al. (2018) The corticostriatal adenosine A(2A) receptor controls maintenance and retrieval of spatial working memory. Biol Psychiatry 83: 530–541.

Lopes LV, Cunha RA, Ribeiro JA (1999) Cross talk between A(1) and A(2A) adenosine receptors in the hippocampus and cortex of young adult and old rats. J Neurophysiol 82:3196–3203.
Lopes CR, Goncalves FQ, Olaio S, Tome AR, Cunha RA, Lopes JP (2023) Adenosine A(2A) receptors shut down adenosine A(1) receptor-mediated presynaptic inhibition to promote implementation of hippocampal long-term potentiation. Biomolecules 13:715.
Luscher C, Jan LY, Stoffel M, Malenka RC, Nicoll RA (1997) G protein-coupled inwardly rectifying K+ channels (GIRKs) mediate postsynaptic but not presynaptic transmitter actions in hippocampal neurons. Neuron 19:687–695.
Marx M, Feldmeyer D (2013) Morphology and physiology of excitatory neurons in layer 6b of the somatosensory rat barrel cortex. Cereb Cortex 23: 2803–2817.
Marx M, Gunter RH, Hucko W, Radnikow G, Feldmeyer D (2012) Improved biocytin labeling and neuronal 3D reconstruction. Nat Protoc 7:394–407.
Massimini M, Huber R, Ferrarelli F, Hill S, Tononi G (2004) The sleep slow oscillation as a traveling wave. J Neurosci 24:6862–6870.
Mendizabal-Zubiaga JL, Reblet C, Bueno-Lopez JL (2007) The underside of the cerebral cortex: layer V/VI spiny inverted neurons. J Anat 211: 223–236.
Mercer A, West DC, Morris OT, Kirchhecker S, Kerkhoff JE, Thomson AM (2005) Excitatory connections made by presynaptic cortico-cortical pyramidal cells in layer 6 of the neocortex. Cereb Cortex 15:1485–1496.
Miller MN, Okaty BW, Nelson SB (2008) Region-specific spike-frequency acceleration in layer 5 pyramidal neurons mediated by Kv1 subunits. J Neurosci 28:13716–13726.
Mitchell AS, Baxter MG, Gaffan D (2007) Dissociable performance on scene learning and strategy implementation after lesions to magnocellular mediodorsal thalamic nucleus. J Neurosci 27:11888–11895.
Mitchell JB, Lupica CR, Dunwiddie TV (1993) Activity-dependent release of endogenous adenosine modulates synaptic responses in the rat hippocampus. J Neurosci 13:3439–3447.
Mitric M, Seewald A, Moschetti G, Sacerdote P, Ferraguti F, Kummer KK, Kress M (2019) Layer- and subregion-specific electrophysiological and morphological changes of the medial prefrontal cortex in a mouse model of neuropathic pain. Sci Rep 9:9479.
Moore KA, Nicoll RA, Schmitz D (2003) Adenosine gates synaptic plasticity at hippocampal mossy fiber synapses. Proc Natl Acad Sci U S A 100: 14397–14402.
Neske GT (2015) The slow oscillation in cortical and thalamic networks: mechanisms and functions. Front Neural Circuits 9:88.
Nguyen MD, Lee ST, Ross AE, Ryals M, Choudhry VI, Venton BJ (2014) Characterization of spontaneous, transient adenosine release in the caudate-putamen and prefrontal cortex. PLoS One 9:e87165.
Oniz A, Inanc G, Taslica S, Guducu C, Ozgoren M (2019) Sleep is a refreshing process: an fNIRS study. Front Hum Neurosci 13:160.
Ouhaz Z, Fleming H, Mitchell AS (2018) Cognitive functions and neurodevelopmental disorders involving the prefrontal cortex and mediodorsal thalamus. Front Neurosci 12:33.
Parnavelas JG, Lieberman AR, Webster KE (1977) Organization of neurons in the visual cortex, area 17, of the rat. J Anat 124:305–322.
Pichon F, Nikonenko I, Kraftsik R, Welker E (2012) Intracortical connectivity of layer VI pyramidal neurons in the somatosensory cortex of normal and barrelless mice. Eur J Neurosci 35:855–869.
Porkka-Heiskanen T, Kalinchuk AV (2011) Adenosine, energy metabolism and sleep homeostasis. Sleep Med Rev 15:123–135.
Porkka-Heiskanen T, Strecker RE, Thakkar M, Bjorkum AA, Greene RW, McCarley RW (1997) Adenosine: a mediator of the sleep-inducing effects of prolonged wakefulness. Science 276:1265–1268.
Qi HX, Jain N, Preuss TM, Kass JH (1999) Inverted pyramidal neurons in chimpanzee sensorimotor cortex are revealed by immunostaining with monoclonal antibody SMI-32. Somatosens Mot Res 16:49–56.
Qi G, van Aerde K, Abel T, Feldmeyer D (2017) Adenosine differentially modulates synaptic transmission of excitatory and inhibitory microcircuits in layer 4 of rat barrel cortex. Cereb Cortex 27:4411–4422.
Quiroz C, et al. (2009) Key modulatory role of presynaptic adenosine A2A receptors in cortical neurotransmission to the striatal direct pathway. Sci World J 9:1321–1344.
Rainnie DG, Grunze HC, McCarley RW, Greene RW (1994) Adenosine inhibition of mesopontine cholinergic neurons: implications for EEG arousal. Science 263:689–692.
Reblet C, Lopez-Medina A, Gomez-Urquijo SM, Bueno-Lopez JL (1992) Widespread horizontal connections arising from layer 5/6 border inverted cells in rabbit visual cortex. Eur J Neurosci 4:221–234.
Rebola N, Lujan R, Cunha RA, Mulle C (2008) Adenosine A2A receptors are essential for long-term potentiation of NMDA-EPSCs at hippocampal mossy fiber synapses. Neuron 57:121–134.
Rebola N, Pinheiro PC, Oliveira CR, Malva JO, Cunha RA (2003) Subcellular localization of adenosine A(1) receptors in nerve terminals and synapses of the rat hippocampus. Brain Res 987:49–58.
Ribeiro JA, Sebastiao AM, de Mendonca A (2002) Adenosine receptors in the nervous system: pathophysiological implications. Prog Neurobiol 68:377–392.
Rombo DM, Dias RB, Duarte ST, Ribeiro JA, Lamsa KP, Sebastiao AM (2016) Adenosine A1 receptor suppresses tonic GABAA receptor currents in hippocampal pyramidal cells and in a defined subpopulation of interneurons. Cereb Cortex 26:1081–1095.
Rombo DM, Newton K, Nissen W, Badurek S, Horn JM, Minichiello L, Jefferys JG, Sebastiao AM, Lamsa KP (2015) Synaptic mechanisms of adenosine A2A receptor-mediated hyperexcitability in the hippocampus. Hippocampus 25:566–580.
Romo R, Brody CD, Hernandez A, Lemus L (1999) Neuronal correlates of parametric working memory in the prefrontal cortex. Nature 399:470–473.
Simoes AP, Machado NJ, Goncalves N, Kaster MP, Simoes AT, Nunes A, Pereira de Almeida L, Goosens KA, Rial D, Cunha RA (2016) Adenosine A(2A) receptors in the amygdala control synaptic plasticity and contextual fear memory. Neuropsychopharmacology 41:2862–2871.
Steger RM, Ramos RL, Cao R, Yang Q, Chen CC, Dominici J, Brumberg JC (2013) Physiology and morphology of inverted pyramidal neurons in the rodent neocortex. Neuroscience 248:165–179.
Steriade M (2000) Corticothalamic resonance, states of vigilance and mentation. Neuroscience 101:243–276.
Strecker RE, Morairty S, Thakkar MM, Porkka-Heiskanen T, Basheer R, Dauphin LJ, Rainnie DG, Portas CM, Greene RW, McCarley RW (2000) Adenosinergic modulation of basal forebrain and preoptic/anterior hypothalamic neuronal activity in the control of behavioral state. Behav Brain Res 115:183–204.
Thompson SM, Haas HL, Gahwiler BH (1992) Comparison of the actions of adenosine at pre- and postsynaptic receptors in the rat hippocampus in vitro. J Physiol 451:347–363.
Thomson AM (2010) Neocortical layer 6, a review. Front Neuroanat 4:13.
van Aerde KI, Feldmeyer D (2015) Morphological and physiological characterization of pyramidal neuron subtypes in rat medial prefrontal cortex. Cereb Cortex 25:788–805.
van Calker D, Biber K (2005) The role of glial adenosine receptors in neural resilience and the neurobiology of mood disorders. Neurochem Res 30:1205–1217.
Verweij IM, Romeijn N, Smit DJ, Piantoni G, Van Someren EJ, van der Werf YD (2014) Sleep deprivation leads to a loss of functional connectivity in frontal brain regions. BMC Neurosci 15:88.
Wall MJ, Richardson MJ (2015) Localized adenosine signaling provides fine-tuned negative feedback over a wide dynamic range of neocortical network activities. J Neurophysiol 113:871–882.
Wang S, Kurada L, Cilz NI, Chen X, Xiao Z, Dong H, Lei S (2013) Adenosinergic depression of glutamatergic transmission in the entorhinal cortex of juvenile rats via reduction of glutamate release probability and the number of releasable vesicles. PLoS One 8:e62185.
Ward JH (1963) Hierarchical grouping to optimize an objective function. J Am Stat Assoc 58:236–244.
West DC, Mercer A, Kirchhecker S, Morris OT, Thomson AM (2006) Layer 6 cortico-thalamic pyramidal cells preferentially innervate interneurons and generate facilitating EPSPs. Cereb Cortex 16:200–211.
Wu LG, Saggau P (1994) Adenosine inhibits evoked synaptic transmission primarily by reducing presynaptic calcium influx in area CA1 of hippocampus. Neuron 12:1139–1148.
Wu LG, Saggau P (1997) Presynaptic inhibition of elicited neurotransmitter release. Trends Neurosci 20:204–212.
Yang SC, Chiu TH, Yang HW, Min MY (2007) Presynaptic adenosine A1 receptors modulate excitatory synaptic transmission in the posterior piriform cortex in rats. Brain Res 1156:67–79.
Yang C, Franciosi S, Brown RE (2013) Adenosine inhibits the excitatory synaptic inputs to basal forebrain cholinergic, GABAergic, and parvalbumin neurons in mice. Front Neurol 4:77.
Yang D, Qi G, Ding C, Feldmeyer D (2022) Layer 6A pyramidal cell subtypes form synaptic microcircuits with distinct functional and structural properties. Cereb Cortex 32:2095–2111.

Yang CR, Seamans JK, Gorelova N (1996) Electrophysiological and morphological properties of layers V-VI principal pyramidal cells in rat prefrontal cortex in vitro. J Neurosci 16:1904–1921.

Yoon KW, Rothman SM (1991) Adenosine inhibits excitatory but not inhibitory synaptic transmission in the hippocampus. J Neurosci 11:1375–1380.

Zhang P, Bannon NM, Ilin V, Volgushev M, Chistiakova M (2015) Adenosine effects on inhibitory synaptic transmission and excitation-inhibition balance in the rat neocortex. J Physiol 593:825–841.

Zhang ZW, Deschênes M (1997) Intracortical axonal projections of lamina VI cells of the primary somatosensory cortex in the rat: a single-cell labeling study. J Neurosci 17:6365–6379.